Constraining the timing of brittle deformation and sedimentation in southern Finland : Implications for Neoproterozoic evolution of the eastern Fennoscandian shield

Elminen, Tuija

2018-01

Elminen , T , Zwingmann , H & Kaakinen , A 2018 , ' Constraining the timing of brittle deformation and sedimentation in southern Finland : Implications for Neoproterozoic evolution of the eastern Fennoscandian shield ' , Precambrian Research , vol. 304 , pp. 110-124 . https://doi.org/10.1016/j.precamres.2017.10.014

http://hdl.handle.net/10138/308825
https://doi.org/10.1016/j.precamres.2017.10.014

Constraining the timing of brittle deformation and sedimentation in southern Finland: Implications for Neoproterozoic evolution of the eastern Fennoscandian shield

*Tuija Elminen[a], Horst Zwingmann[b], Anu Kaakinen[c]

[a]Geological Survey of Finland GTK, P.O. Box 96, FI-02151 Espoo, Finland

[b]Department of Geology and Mineralogy, Graduate School of Science, Kitashirakawa Oiwakecho, Sakyo-ku, Kyoto University, Kyoto, 606-8502, Japan

[c]Department of Geosciences and Geography, P.O. Box 64, 00014 University of Helsinki, Finland

*Corresponding author

Abstract

Sheared sedimentary clay was found in a faulted fracture in crystalline bedrock in a tunnelling site at 60 m depth in southern Finland. Brittle faults are numerous in the Fennoscandian Palaeoproterozoic bedrock, but only some of them have relative age constraints, while absolute ages are nearly lacking. Sedimentary rocks altogether are uncommon in Finland and only sparsely dated by micropaleontological studies. This study reports K–Ar data of fresh, non-weathered authigenic illite and constrains a time framework for the local faulting and sedimentation. The Neoproterozoic Tonian to

Cryogenian ages derived from the grains in diminishing grain-size order are c. 967, 947, 809 and 697 Ma. Results indicate that the formation of the extension fracture is related to the collapse of Sveconorwegian orogeny c. 1000 Ma; clay and mature quartz sand were deposited in this extension fracture in shallow water in an intracratonic basin followed by early diagenetic processes and neocrystallization of illite around 967–947 Ma. The Neoproterozoic 1000–700 Ma sedimentation documented in this study is rare in the Fennoscandian shield as a whole. Neocrystallization of authigenic illite in the finest 0.4 and <0.1 μm fractions c. 809–697 Ma ago is interpreted as resulting from reactivation in the fault due to the continental break-up on the western side of the craton as documented by arenite crosscutting relationships. The younger ages may also be attributed to a Caledonian thermal overprint ca. 410 Ma ago that would influence the 967 Ma age if sufficient thermal energy had been present.

Keywords: Clay, fault, K-Ar dating, Neoproterozoic, thermal event, Sveconorwegian orogeny

1. Introduction

Constraining the timing of fault zone formation is of geotectonic importance to understand structural evolutions and brittle fault processes. Early studies by Lyons and Snellenberg (1971) highlighted the applicability of isotopic dating techniques in constraining the age of brittle faults, and numerous isotopic approaches have since been applied, including the K–Ar method (e.g. Kralik et al., 1992; Vrolijk and van der Pluijm, 1999; Choo and Chang,

2000; Zwingmann and Mancktelow, 2004; Sasseville et al., 2008; Zwingmann et al., 2010a, b; Zwingmann et al., 2011; Pleuger et al., 2012; Hetzel et al., 2013; Viola et al., 2016), the ^{40}Ar–^{39}Ar method (e.g. van der Pluijm et al., 2001; Solum et al., 2005; Haines and van der Plujim, 2008; Duvall et al., 2011) and the Rb/Sr method (Kralik et al., 1987; 1992). Viola et al. (2013) extended this approach to date complex brittle faults in the Palaeoproterozoic basement of southwestern Finland aiming at also directly dating fault reactivation.

Brittle faulting is ubiquitous in the Fennoscandian basement, but the common lack of dated sedimentary marker horizons makes it difficult to constrain absolute timing or link the faults to specific geological events. Only limited absolute ages from a few locations have been reported in the literature. In Forsmark in central Sweden fracture fillings related to brittle deformation and hydrothermal events have been dated yielding ^{40}Ar–^{39}Ar ages of 1.8–1.7 Ga that can be interpreted as dating the brittle-ductile transition, in addition to 1107±7 – 1034±3 Ma and several Palaeozoic ages in the brittle realm (Sandström et al., 2009; Fig. 1; Fig. 2). In southern Finland, ^{40}A–^{39}Ar geochronometry has been applied to the Porkkala–Mäntsälä fault (Heeremans and Wijbrans, 1999), which is a major polyphase shear and fault zone predating the adjacent c. 1645 Ma (Vaasjoki, 1977a) Obbnäs rapakivi granite. Fault generations crosscutting the rapakivi provided ages predominantly in the 1300 – 950 Ma range (Heeremans and Wijbrans, 1999). Viola et al. (2013) reported illite K–Ar ages (1006.2 ± 20.5 Ma and 885.8 ±18.3 Ma) from <0.1µm fractions from a single but reactivated gouge fault in a drill core from SW Finland. Palaeozoic faulting documented at 445 ± 9 Ma has been discussed by Torgersen et al. (2014) in northern Norway along the edge of a Palaeoproterozoic tectonic window in close proximity to the Caledonides. To summarise, the framework of brittle faulting within the Fennoscandian

shield remains limited leaving the timescales and formation history of most of the brittle structures still obscure.

The Finnish Palaeoproterozoic bedrock is mostly veneered by unconsolidated deposits of Quaternary age, which are the results of glacial and glaciofluvial depositional processes. Only a few sedimentary rock occurrences of Mesoproterozoic age exist in the Satakunta and Muhos grabens (e.g. Kohonen and Rämö, 2005; Fig. 1), and these formations extend into the Gulf of Bothnia (Winterhalter et al., 1981; Fig. 2). Minor Neoproterozoic to Palaeozoic deposits have been documented from some impact craters (Tynni, 1978; Elo et al., 1993; Pesonen et al., 1998) and as fissure fillings (Bergman, 1982). The closest known occurrences of sedimentary rocks to the study area are sedimentary dykes in the southern archipelago, approximately 115 km to the SW (Pokki, 2006).

In this study, we report K–Ar ages of a previously unreported 30-cm-wide sedimentary clay infill of a faulted fracture that was found within a tunnel site in southern Finland. The ages provide constraints for the local and regional faulting events and sedimentation at the site. The sample of the clay deposit cannot have been subject to weathering, because it was collected from a fresh deep tunnel site (see a similar approach reported by Zwingmann et al., 2010a; Yamasaki et al., 2013), and there are independent thermochronological constraints on the possible age range for the formation of the fault.

2. Geological background

88 The bedrock in southern Finland is part of the Fennoscandian Shield, consisting of 1.9–1.8
89 Ga Palaeoproterozoic Svecofennian rocks (e.g. Koistinen et al., 1996) (Fig. 1). The study
90 area is situated within the Uusimaa belt (Vaasjoki et al., 2005). Amphibolite facies
91 supracrustal rocks comprise mica gneisses, quartz-feldspar gneisses, amphibolites and
92 carbonate rocks, intruded by plutonic rocks during several tectonic phases. In the study
93 area, foliated tonalites and granodiorites dominate and coarse-grained granitic pegmatites
94 are abundant. Migmatization is strong and lithological units frequently alternate. The
95 dominant NE–SW structural grain formed in a transpressional tectono-thermal stage at
96 1.87–1.80 Ga (Pajunen et al., 2008).

97 The bedrock was peneplaned by 1650–1630 Ma, when anorogenic rapakivi plutons and
98 related dykes intruded the crust (Laitakari et al., 1996). The closest pluton (Bodom), which
99 is located 13 km to the west of the study area, has been dated by the zircon U-Pb to 1645 ±
100 12 Ma (Vaasjoki, 1977). A 1632 ± 9 Ma (Törnroos, 1984) granite porphyry dyke is situated
101 7.7 km from the study site, and during the mapping of the tunnel, new diabase and quartz
102 porphyry dykes of the same orientation and probably same age group were identified 2 km
103 from the tunnel site (Elminen et al., 2007).

104 The oldest non-metamorphic sedimentary rocks in Finland are Mesoproterozoic clastic
105 sediments located in the Satakunta and Muhos grabens (Fig. 1). The Satakunta sandstone
106 formation with fluvial arkose arenite as the main component is crosscut by 1270–1250 Ma
107 diabases (Suominen, 1991) and underwent a complex multiple basin development starting
108 at c. 1600 Ma (Pokki et al. 2013; Mattila and Viola, 2014). The Muhos shales document
109 sedimentation between 1400–1300 Ma ago as documented by K–Ar and Rb–Sr dating from
110 the shale (Simonen, 1980). Formation ages for the graben have not been defined. Also 300

km to East in Russia, in a graben-like structure of Lake Ladoga, sedimentary rocks from at least Middle Riphean to Early Vendian (c. 1400–650 Ma) are documented and the older sequences are cut by mafic intrusions of 1250–1200 and 1100 Ma (Amantov et al., 1995; Fig. 1A). Dated Mesoproterozoic to Neoproterozoic sedimentary rocks and brittle faults in Finland and some parts of Fennoscandian shield are compiled in Fig. 2.

Neoproterozoic ages for the sedimentary rocks have only been estimated from micropaleontological studies, providing so far only relative age constrains. The Hailuoto formation, which outcrops on the Hailuoto Island in the Gulf of Bothnia, is geographically close to the Muhos formation and comprises conglomerates, sandstones and mudstones, the latter containing acritarch forms and blue-green algae of the filamentous type. Tynni and Donner (1980) suggested the age of the Hailuoto formation to be about 600 Ma based on microfossils, although older ages are possible. Comparable microfossils of possibly the same age have been observed in the Taivalkoski formation (Tynni and Uutela, 1985), located in the Saarijärvi impact crater 160 km to the east (Pesonen et al., 1998). The formation consists of alternating clay/shale and sandstone layers (Hyyppä and Pekkala, 1987). Another assumed impact crater with Neoproterozoic sediments is in Lake Iso-Naakkima, where micropaleontological studies have suggested sedimentation between 1000 and 650 Ma in a fluvial and lacustrine or lagoonal environment. The sedimentary succession contains conglomerates, sandstones, siltstones, shale and kaolinitic clay (Elo et al., 1993).

Some younger sedimentary dykes occur on the islands of the Archipelago Sea, west of the study area (Bergman, 1982) (Fig. 1b). The dykes in Åland are usually curved and strike N 0-20 E, dips are vertical and the material varies from quartz arenite to arkose arenite (Bergman, 1982). The fossils in Åland dykes document various early Palaeozoic ages, from lower Cambrian to Middle Ordovician (Tynni, 1982).

3. Study site and material

An extension fracture with sedimentary clay in it was discovered underground during the excavation of a railway tunnel at Myras, at the Savio railway tunnel site in Vantaa, c. 25 km north of Helsinki (Fig. 1; N 60° 19.463', E 25° 6.95'). The bedrock above the tunnel has a thickness of 20 m and is in turn overlain by 35 m of Quaternary sediments. The bedrock is intensely fractured at the site, and because of geotechnical reasons and urgent tunnel stabilization, only a brief examination of the clay was possible. Additional measurements of the fault were, however, carried out by the consulting company Pöyry. The host rocks at the site contain granite, granite pegmatite and veined mica gneiss.

The clay-decorated N20E striking fracture is located at 20 m distance from a 30 m wide N45E mylonite shear zone (Fig. 3a). The ductile- semiductile mylonite is crosscut by four 2–20-cm-thick steep to moderate dipping incohesive and cohesive cataclasites, striking N41-70E. The mylonite is intensely fractured and partly altered as documented by sericite, chlorite, and Fe oxide minerals. This N45E striking fault zone can be distinguished in magnetic data set as a low magnetic anomaly continuing 11 km to the SW, discontinuously even 30 km. In topographical data, the same lineament is evidenced by a depression or step

154 in some parts along this anomaly. The depression is covered by Quaternary sediments and
155 some places a mire. There are two mylonite observations on the outcrops next to the
156 anomaly in the coast.

157

158 3.1 Sediment deposit

159 The clay deposit in the extension fracture was examined in the tunnel and in two drill cores
160 (Fig. 3) drilled before excavation. The strike of the clay-filled fracture is N20E and the dip
161 is 75° to SE, and it could be traced on the floor of the tunnel as a 30- to 70-cm-thick
162 undulating zone of unconsolidated clay. The contact zone between the sediment and the
163 bedrock could not be observed because of mud on the tunnel floor and ongoing
164 construction work. The clay contained variable proportions of sand-sized clasts and was
165 moist and mouldable at the time of excavation, drilling and at the micropaleontological
166 study, but dry at the time of other laboratory examinations. The colour was mainly greenish
167 grey (air-dry Munsell ® colour Gley 1 7/1; light greenish grey) (Fig. 4a), but in places it
168 was red (air-dry Munsell ® colour 10R 5/4 – 4/4; weak red) and the sediment had a sheared
169 appearance.

170

171 In the eastern contact, the clay deposit that outcropped in the tunnel, was cut by a parallel
172 5-cm-thick white quartz arenite-filled fissure cemented by carbonate and containing grey,
173 silicified clay inclusions (Fig. 4b). Slickenlines on the clay along the contact to the arenite
174 indicate east side down normal faulting. The clay sample for the study was taken from the

tunnel floor (Fig. 3a). An arenite sample was taken from the wall from the height of one metre.

Two drill cores, SK5067 and SK5037, dipping c. 45°, intercept the clay deposit. (Fig. 3). Core SK5067 crosscuts the deposit 3 m above the tunnel floor at 45 m distance from the tunnel sampling point. The width of the clay-rich zone in the core is approximately 40 cm. Within this zone, about 5–10 cm of sheared and mixed clay and rock material borders the sediment sequence on both sides. The vertical tilt-corrected thickness of the sediment sequence is about 60 cm. The sequence starts with red clay, overlain by a sharp contact with a white carbonate-cemented quartz arenite showing bedding structures (Fig. 5a). The sequence is capped by red clay containing grey patches. The individual units are 20–25 cm thick. The rock around the sediment sequence is a fractured and altered granitic rock.

Core SK5037 intercepts the clay deposit 15 m above the tunnel floor outside the tunnel, also c. 45 m north of the sampling point, and it contains a 4.8-m-thick sequence of clay-rich deposits (tilt corrected). The dip direction of the drill core is close to the fault strike. The sediments overlying the altered bedrock include a 20-cm-thick bed of sheared clay (Fig. 5b) containing lithic fragments up to 3 cm, and a decimetre-thick bed of siltstone. The remaining succession is dominated by pale white sheared clay rich in randomly oriented lithic fragments, capped above and below by thicker units of red clay.

4. Methods

196 4.1 K-Ar sample preparation

197 The procedures applied in this study are based on Zwingmann et al. (2010a).
198 Approximately 200 g of fresh clay material was collected from the tunnel sample site. The
199 sample was gently disaggregated using a repetitive freezing and heating technique to avoid
200 artificial reduction of rock components with K-bearing minerals, such as micas or K-
201 feldspars (Liewig et al. 1987). Grain size fractions <2 and 2–6 μm were separated in
202 distilled water according to Stoke's law, and <0.4 and <0.1 μm fractions were separated
203 using a high-speed centrifuge. Samples were characterized by X-ray diffraction (XRD,
204 normal and glycolated runs), scanning electron microscopy (SEM) and transmission
205 electron microscopy (TEM).

206

207 4.2. Mineralogy

208 For XRD analysis, a Philips X-Pert MPD X-ray diffractometer with a Cu tube operated at
209 40 kV and 55 mA was used. The step size was 0.02° 2Θ and the time per step 1.00 s.
210 Randomly oriented bulk clay samples were analysed to characterize all the mineral phases
211 in the sample. They were scanned at an interval of 2–70° 2Θ. Oriented samples were
212 prepared to specify the clay minerals. The finest fraction was sedimented onto glass slides
213 (grain size <2 μm) and air-dried. Ethylene glycol was added to one of the oriented samples
214 to test the swelling properties of possible clay minerals. Another oriented sample was
215 heated at 550 °C for 1 h. They were scanned at an interval of 2–20° 2 Θ. Minerals were
216 identified using HighScore Plus software by PANalytical with the ICDD (International
217 Center for Diffraction Data) mineral database PDF-4/minerals 2010. Infrared

218 spectrophotometer (IR) analysis was obtained from the material in support of the XRD
219 analysis. The prepared sample was analysed with a Perkin Elmer 983 G instrument using
220 KBr as flux material.

221

222 4.3. Petrography

223 The bulk dry clay crumbs and the coarse fraction of the clay were examined with a JEOL
224 JSM 5900 LV SEM equipped with an attached EDS (energy dispersive X-ray system,
225 Oxford Instruments) analyser. SEM petrography was used for identifying minerals and for
226 examining the surface structures of the quartz grains. Dry clay crumb samples were coated
227 with gold, and a coarse fraction was additionally investigated without coating. INCA Point
228 ID software was used for mineral identification. The arenite samples were investigated in
229 thin sections via a conventional petrographic microscope and using an electron probe
230 microanalyser (Cameca SX100).

231 Transmission electron microscopy (TEM) was used to identify and distinguish possible
232 authigenic clays from finely ground protolith micas, feldspars and other fine grained clay
233 minerals, allowing the detection of traces of potential contaminantion phases below the
234 XRD detection limit. A JEOL 2010 TEM (200 KV) was used for detailed, grain-by-grain
235 morphological characterization of the <0.1 μm clay fraction. The sample was prepared by
236 placing one drop of clay solution on a micro-carbon grid film and drying under air. The
237 chemical composition of individual particles was investigated by an attached EDS system.

238

4.4 K–Ar dating

The K–Ar dating technique followed standard methods described in detail by Dalrymple and Lanphere (1969). The K content was determined by atomic absorption. The pooled error of duplicate K determinations on several samples and standards was better than 2.0%. Ar isotopic determinations were performed using a procedure similar to that described by Bonhomme et al. (1975). Samples were pre-heated under vacuum at 80 °C for several hours to reduce the amount of atmospheric Ar adsorbed onto the mineral surfaces during sample preparation. Blanks for the extraction line and mass spectrometer were systematically determined and the mass discrimination factor was determined by airshots. About 10 mg of sample material was required for Ar analyses. Due to the hygroscopic nature of clays, special care was taken in the preparation of both K and Ar sample splits. For Ar analysis by noble gas spectrometry, sample splits were loaded onto clean Mo foil (Goodfellow molybdenum foil, thickness 0.0125 mm, purity 99.9%), weighed and subsequently preheated to 80 °C overnight to remove moisture, and re-weighed using a Mettler AT20 balance. The measured dry weight was used in the K–Ar age calculation. Samples were stored prior to loading into the Ar purification line in a desiccator. During the analysis, one international standard HD-B1 (Hess and Lippolt, 1994) was measured. The error for Ar analyses was below 1.00% (Table 1) and the $^{40}Ar/^{36}Ar$ value for airshots averaged 295.02 ± 0.28 (n = 2). The standard and airshot data are presented in Table 1. The K–Ar ages were calculated using ^{40}K abundance and decay constants recommended by Steiger and Jäger (1977).

4.5 Grain size and microfossils

The grain-size distributions in the size range of 0.15–2000 μm were determined for selected samples using a Malvern 2000 laser particle sizer. The fresh sample was analysed for microfossils by treating with acid extraction and sodium metatungstate solution, but the material was devoid of carbonaceous fossils. However the circumstances at the time of sedimentation or later may not have been favorable for the microfossils to be preserved and constraining the sedimentary origin and age by microfossils was not possible.

5. Results

5.1. Mineralogy of the clay and arenite samples

The bulk clay sample was found to consist of illite, quartz, K-feldspar and chlorite (Table 2). The median grain sizes of the clay sample varied between ca. 1 and 7.5 μm, and all were found to be poorly sorted with a distinct sand fraction mainly consisting of rounded quartz grains with small proportions of angular grit (Fig. 6). The decanted coarse fraction was dominated by quartz with a lesser amount of K-feldspar, chlorite and illite.

The modal mineral composition determined by XRD of the <2 μm clay size fractions dated in this study is summarized in Table 2. This fraction was found to contain 42% 2M1 illite (high temperature polytype), 54% 1M illite (low temperature polytype) and 5% chlorite. Due to the low amount of separated clay material from the <0.1 and <0.4 μm fractions, no XRD analyses were obtained from these fractions.

281 Typical SEM and TEM images are illustrated in Fig. 7. Sample characterization by SEM
282 and TEM suggests that most illite crystallites have a preferred orientation and exhibit
283 euhedral shapes (Fig. 7). The fibrous and hexagonal and prismatic morphologies of the
284 illite particles suggest *in situ* neocrystallization (Clauer and Chaudhuri, 1995) but cannot be
285 related to polytypes.

286 The arenite sample mainly consists of well-sorted and well-rounded quartz grains cemented
287 by calcite exhibiting compositional and textural maturity (Fig. 8a). Feldspar and muscovite
288 grains, a rounded illite grain and glauconite, both as a grain and cement are as minor
289 constituents (Fig. 8b). A silicified clay chip with some illite remnants is also present in the
290 studied thin section (EPMA) (Figs 8a, c). A microscopic cataclasite cemented by calcite
291 crosscuts the arenite sample (Fig. 8d).

292

293 5.2 K-Ar dating

294 In total, four K-Ar analyses of clay fractions from <0.1 to 2–6 μm were obtained in this
295 study (Table 3, Fig. 7. The ages of the clay fractions range from 697.3 ± 14.1 to 967.6 ±
296 19.7 Ma. A decrease in age with decreasing grain size is observed (Fig. 9). A total age span
297 of 270 Ma is recorded within the clay fractions, ranging from the Neoproterozoic-
298 Cryogenian for the finer <0.1 and <0.4 μm fraction to the Neoproterozoic-Tonian for the
299 coarser <2 and 2–6 μm fractions. The relatively high K content of the clay fractions,
300 ranging from 6.40 to 6.78%, is consistent with a potential authigenic origin (Clauer and
301 Chaudhuri, 1995; Aronson and Hower, 1976). The radiogenic ^{40}Ar content ranges from

97.8 to 99.2%, indicating reliable analytical conditions for all analyses with no significant atmospheric ^{40}Ar contamination. Ages refer to the timescale of Gradstein et al. (2004).

6. Discussion

Fault gouges are common in rock cuts and widely reported in Fennoscandia but sedimentary clay filled fissures have not been identified so far in Finland. The unusual homogeneity in a 30-cm-wide clay zone and an uncommon arenite fissure in close proximity suggest preservation of a sedimentary deposit instead of a gouge. The sand-sized clasts in the clay consist of well-rounded quartz confirming a sedimentary origin as well as the arenite sections in the drill cores. The clay resembles post glacial clays that are ubiquitous in Fennoscandia but quartz grains in the clay and the arenite that post-dates the clay are more mature compared to the Quaternary sediments and suggest a deposition in a different and older environment.

The sharp-edged broken grains and the slicken-lines in the clay, sheared clay in the drill core and brecciated arenite are an evidence of later reactivations in the fissure and suggest faulting. The clay fraction morphology investigated by TEM indicates an authigenic origin and the obtained age interval can be interpreted to record the time of illite formation after deposition.

6.1 Clay fraction ages

Grain-size fractions of authigenic illite can contain mixtures of illite particles formed at different times during growth, and this growth history is usually investigated by K-Ar

323 dating a range of different grain-size fractions. Similarly to other fault-dating studies (for
324 example Solum et al., 2005; Haines and van der Pluijm, 2008; Sasseville et al., 2008;
325 Zwingmann et al., 2010a, b; Viola et al., 2013, 2016), we observed a clear age distribution
326 of the grain size, with the smallest <0.1 µm fraction yielding the youngest age at 697.3
327 ±14.1 Ma. The ages increase to 809.3 ± 16.4 Ma for the <0.4 µm fraction and 947.1 ± 19.5
328 Ma for the <2 µm fraction. The oldest age is from the coarse-grained 2–6 µm fraction, at
329 967.6 ± 19.7 Ma, which is almost identical within error to the obtained <2 µm fraction. As
330 discussed by Zwingmann et al. (2010a) for neocrystallized illite, the finest separated
331 particle size is often derived from the ends of filamentous grains and represents the most
332 recently grown illite in the gouge rocks. Coarser size fractions are normally formed earlier
333 during the illite formation process, yielding older ages.

334 Dating authigenic clay mineral crystallization involves a fundamentally different approach
335 from dating detrital clays (Meunier et al. 2004). As summarized by Zwingmann and
336 Mancktelow (2004) the dating of clay minerals involves the assumption that a newly
337 formed authigenic clay mineral can be dated by isotopic techniques independent of the
338 concept of a closure temperature. This crystallization process can encompass different
339 timescales. If the time interval over which an authigenic mineral has crystallized is shorter
340 than the analytical precision of the method, described in 1 or 2 sigma values, an actual
341 "age" is recorded. However, in some geological case studies, mineral authigenesis and
342 crystallization can extend over extensive time periods, larger than the analytical
343 uncertainties, and an "integrated age" is recorded (Meunier et al., 2004).
344

345 6.2 Brittle fault succession in Myras area

346 The brittle faults and their relative ages and kinematics have been studied in an area of c. 60
347 km x 60 km, where Myras site also is located (Elminen et al., 2008). The fault sets
348 comprise:

349 (1) Steep NE-trending ductile shear zones (Figs. 1b, 10a), formed in the latest stages of
350 Svecofennian orogeny (Pajunen et al., 2008). The NE-trending structural lines in Fig. 1b
351 indicate these major shear zones. Sinistral E-side-up reverse movement is recorded in the
352 mylonite structures in retrograde conditions (Elminen et al., 2008). Väisänen and Skyttä
353 (2007) conclude that these shear zones were formed between 1.81 and 1.79 Ga. The zones
354 have been reactivated later in brittle conditions shown by cataclasites. The 50-m-wide
355 ductile-semiductile mylonite close to the studied clay-filled extension fracture corresponds
356 to this Late Svecofennian event. (Figs. 3a, 10a)

357 (2) During the anorogenic rapakivi magmatism and its related dykes (ca. 1640 Ma) dextral
358 strike-slip reactivation occurred along the pre-existing NE-shear zones in brittle conditions
359 as well as new brittle NE strike-slip faults were formed (Elminen et al., 2008; Fig. 10b).
360 Shearing is observed in the edge of the cooling Bodom rapakivi pluton edge along one of
361 the major faults, Porkkala-Mäntsälä fault (PM in Fig. 1b and 10b). These faults and the
362 NW-SE-oriented diabase dykes document a regime where the major principal stress axis
363 was oriented NW-SE and minor principal stress axis approximately NE-SW. The NW-SE
364 normal faults crosscutting rapakivi granites have still formed in same stress field. (Fig. 10b)

365 (3) Vertical N-S-trending faults further crosscut the previous NE- and NW-trending faults
366 (Fig. 10c) and they exhibit sinistral strike-slip (Elminen et al., 2008). The shortening axis is
367 approximately NW-SE oriented in the paleostress field. Reactivation on the previous NW-

368 fault planes at the same time as N-S fault formation is likely. No age constrains is available
369 in the literature.

370 The NNE-trending clay-filled fracture is kinematically not in concordance with either of the
371 described faulting events. The extensional fracture and normal faulting refer to NNE-SSW
372 shortening axis and ESE-WNW extensional axis (Fig. 10d). The new K-Ar age data with
373 the kinematic indicators suggest that the Myras clay-filled fracture formed in an additional
374 extensional faulting event in southern Finland.

375 Fig. 11 summarizes the interpretation of the obtained illite ages in the complex geological
376 framework of the study area in the Proterozoic within 4 major simplified phases. Phase 1
377 highlights the basement paleostress tensors and related rapakivi plutons and diabase dykes
378 age ranges in S-SE and SW Finland. Phase 2 is interpreted to document a minimum age for
379 the opening of the fracture and sediment deposition with the obtained 2-6 and <2 µm ages
380 at ca. 967.6 ± 19.7 to 947.1 ± 19.5 Ma, which are identical within error. These 2-6 and <2
381 µm ages are interpreted to document early diagenetic processes with involved
382 neocrystallization of illite. Opening of the fracture in extensional conditions is consistent
383 with the collapse of the Sveconorwegian orogeny in the West, which is estimated to have
384 commenced 970 Ma (Bingen et al., 2008).

385 Phase 3 documents extension processes with the sand infill, after the initial clay infill. The
386 clay has been compacted before the opening of the smaller fracture where the quartz sand
387 was deposited. The slickenlines in the contact of the clay and arenite show normal faulting,
388 likely after sand infill. Faulting after the sand cementation is documented by brecciated
389 arenite, which was subsequently cemented. The extensional fracturing can be related to

390 normal faulting as illustrated in phase 3 in Fig. 9. These processes are interpreted to be
391 attributable to continuing Sveconorwegian collapse or later extensional faulting in Phase 4.

392 Phase 4 causes final faulting and shearing within the sediment infill material. The finest
393 <0.4 and 0.1 μm illite fractions yield ages around 809.3 ± 16.4 Ma to 697.3 ±14.1 Ma. The
394 coarser <0.4 μm illite fraction is interpreted to document onset of faulting, and the <0.1
395 illite age cessation of faulting. The extensional conditions shown by open fractures and
396 normal faulting probably reflect the initial break-up of the Rodinia supercontinent around
397 800–700 Ma at Baltica (Kumpulainen and Nystuen, 1985), which resulted in extensive
398 faulting and sedimentation over a long time in the Baltica basins (Fig. 9). No other tectonic
399 activity has been recorded at the craton at that time except presumable rifting between 1350
400 and 650 Ma in the far NE passive margin of the craton, which has been more than 1200 km
401 apart from the study area (Roberts and Siedlecka, 2002). Fault reactivations by isostatic
402 movements in the crust due to Cryogenian glaciations could be possible but are difficult to
403 assess.

404 Illite K–Ar dating has also been reported from drill core fault gouges from Olkiluoto, ~ 225
405 km NW of Myras (Viola et al., 2011, 2013) (Fig. 1b). A few centimetres wide fault gouge
406 in a brittle deformation zone that was modelled as a SE dipping low-angle fault trending
407 N75E reflected two deformational phases (Viola et al., 2011). The fraction ages were from
408 c.1240 to 1006 Ma in diminishing fraction size and c. 980–886 Ma for the crosscutting
409 gouge (Fig. 9) Faulting was interpreted to have taken place at 1006.2 ± 20.5 Ma in an E–W
410 shortening stress field and reactivation at 885 ± 18.3 Ma in an ESE–WNW extension (Viola
411 et al., 2013). These faults were linked to the Sveconorwegian orogeny. As seen in Fig. 9,
412 the bigger fractions with older age of Olkiluoto younger sample and Myras sample can be

413 interpreted to record the orogen collapse. Thus two separate studies where illite is of
414 different origin indicate the effects of orogen collapse far from the Sveconorwegian front;
415 Myras situating c. 600 km from there.

416 Numerous brittle faults have been observed in southern Finland, but no absolute age dating
417 has been possible or obtained so far. The unique fresh and unweathered clay from the
418 investigated Savio tunnel site might therefore record the timing of the brittle deformation in
419 this area.
420
421 6.3 Caledonian overprint

422 The Cryogenian age of 697.3 ± 14.1 Ma obtained from the finest <0.1 μm fraction could
423 document neoformation of the illite crystals during fault reactivation. In addition, the
424 fraction might contain detrital mineral phases and could be influenced by contamination. A
425 contamination scenario is unlikely. However, despite sound separation methods this clay
426 fraction was obtained from geological old sediments with potential numerous
427 contamination sources of very old and trace amounts of K rich minerals (K-feldspars)
428 below the detection limit of the XRD method. As discussed by Hamilton et al. (1989, their
429 Fig . 4) traces of very old contamination mineral phases could influence the age value of
430 the <0.1 μm fraction.

431 A few studies have suggested a thermal imprint related to the Caledonian orogeny (490–
432 400 Ma) in the Precambrian basement. The palaeo-sedimentary cover on the present
433 surface in Fennoscandia has been suggested to have caused heating and it would have been
434 strongest during the Caledonian foreland sedimentation (Tullborg et al., 1995). Using $\delta^{18}O$

435 and $\delta^{13}C$, Tullborg et al. (1995) calculated temperatures in Ordovician limestones in
436 Sweden and Norway and concluded that raised temperatures of ca.125 °C persisted for at
437 least 100 Ma due to the burial under 2-4 km thick cover. Fission-track thermochronology
438 similarly suggest >2.5 km thick Devonian sediments in the foreland basin in Sweden
439 thinning to the east (Larson et al., 1999). However, significant temperature effects can be
440 excluded for the Myras site, based on the long distance from the assumed foredeep basin.
441 The sedimentary environment at Myras region was more like in a back-bulge setting in a
442 lower depth and with a thinner sedimentary cover. Murrel (2003) applied apatite fission-
443 track thermochronometry to investigate the low-T thermal history in Finland. According to
444 the results, reheating to 75 °C could be interpreted at 430 Ma. However, AFTA and ZFTA
445 dating remains controversial in Scandinavia, as apatite and zircon fission track data, which
446 are often used to constrain the timing of shallow faulting histories, might be questionable or
447 inconclusive in old and convoluted terranes (Redfield, 2010; Viola et al., 2013).

448 Alm et al. (2005) reported 407 ± 54 Ma Sm-Nd isotope age for fluorite veins in SE Finland,
449 indicating fracturing and hydrothermal activity at that time (Fig. 1). U–Pb analyses of
450 uraninites and allanites in sheared rock in east Uusimaa suggested enrichment of uranium
451 ca. 450 Ma (Vaasjoki et al., 2002). Palaeomagnetic studies also indicate that
452 remagnetization might have taken place around 415 Ma (Mertanen et al., 2008). The
453 formation of fluorite veins (Alm et al., 2005) and remagnetization processes do not require
454 high temperatures, and an influence on or thermal overprinting of the illite ages can
455 therefore be ruled out.

456 Based on the complex geological and unknown thermal history of the study area, a
457 potential thermal overprint on the ages of the illite fractions was evaluated by basic illite Ar

458 diffusion calculations similar to the approach by Zwingmann et al. (2010b). As outlined by
459 these authors, K–Ar dating assumes closed system behaviour, which is not always satisfied
460 in fault rocks. If a mineral is exposed to a given temperature close to or slightly above the
461 formation temperature over a distinct time interval, the system might be affected or even
462 partially or completely reset (Clauer and Chaudhuri, 1995). We evaluated the influence of
463 potential Ar diffusion on the illite fractions by a thermal overprint via a basic Ar diffusion
464 model described by Huon et al. (1993) using four maximum grain sizes comprising 2–6, 2,
465 <0.4 and 0.1 µm, a temperature range from 200 to 350 °C and a time frame of 1My and in
466 addition for a low temperature range from 50 to 150 °C and a time frame of 100 My to
467 investigate a potential influence of a low temperature but long lasting Caledonian thermal
468 overprint. Because the shape of fine-grained clay minerals (fibres vs. plates) will strongly
469 influence diffusion, cylindrical and plane geometric shapes were applied. We used the
470 original parameters listed in Huon et al. (1993, p. 174) in the present study, with Do and Ea
471 values of 6.03 × 10 7 cm^2/s and 40 × 103 cal/mol, respectively (Wijbrans and McDougall,
472 1986).

473 The results of these calculations are summarized in Tables 4, 5 and Fig. 12. The smallest
474 <0.1 µm fractions can be affected by a thermal overprint by up to 64% if the temperature is
475 as low as 200 °C during a 1-My overprint time window (Fig. 12a). A potential thermal
476 overprint on the 2 µm grain-size fraction is negligible if the temperature is 200 °C during 1
477 My (Fig. 12c). In the 300 °C range, Ar diffusion will significantly reduce the ages of the
478 <0.1-µm fraction and reset the illite age after ~0.1 My (Fig. 12a). The 2 µm fraction will, in
479 addition, suffer significant radiogenic ^{40}Ar loss of up to 83% over a 1-My time frame. If the
480 temperature increases to a hypothetical 350 °C, the <0.1 µm fraction would start to

481 recrystallize to muscovite and experience reset and complete Ar loss in short time periods
482 of 0.05 Ma. Calculations indicate that an elevated temperature of 250–350 °C over 0.05–1
483 My would thermally disturb ages of the <0.1 or <0.4 μm illite fractions (Fig. 12d). An
484 elevated and heterogeneous thermal history within the study area could therefore modify
485 the illite ages if secondary heating is persistent for an extended time period of 0.05 to 1 Ma,
486 but the measured illite age data do not document these trends, as the ages of <2 and 2–6 μm
487 illite fractions were found to be identical within error, and the data document an age spread
488 of 112 My between the <0.1 and <0.4 μm fractions. However, with the limited data, we
489 cannot unequivocally conclude whether the <0.1 μm fraction might have been influenced
490 by a thermal overprint or documents the cessation of faulting in the study area. As no
491 influence of a thermal overprint has been documented within the coarser clay fractions, we
492 interpret the <0.1 μm fraction to document the cessation of faulting. A suggested long
493 lasting Caledonian 100 My low temperature 100 and 150 °C overprint was modelled and
494 the diffusion results are summarized in Fig. 12e for a 100 °C temperature range indicating
495 negligible Argon diffusion with only the finest 0.1 μm fraction showing very minor
496 diffusion effects. The results of an increased 150 °C temperature range is summarized in
497 Fig. 12f again indicating negligible diffusion in the coarser 2-6 and <2 μm fractions. The
498 <0.4 μm fraction would experience only very minor Argon diffusion of around 10 %
499 whereas the <0.1 μm fraction could lose up to 40% of its radiogenic Argon. As the obtained
500 illite age data do not show age variations in this range, a potential long lasting low
501 temperature Caledonian thermal overprint seems not to have affected the illite fractions and
502 is not a plausible scenario.

503

504 6.4 Inferences for Neoproterozoic sedimentation

505 The sediments in the fracture are interpreted as resulting from an in-situ deposition instead
506 of a collapse due to the primary sedimentary structures present in the drill-core. Clay-sized
507 glauconite was identified as a common constituent in the arenite samples. The formation of
508 glauconite takes place at a shallow water depth with a low terrigenous sedimentation rate
509 (Porrenga, 1967). Formation takes place during the deposition of sediment, at the water–
510 sediment interface, thus becoming an attractive process for isotopic dating of the deposition
511 time of sedimentary rocks (i.e. Odin, 1975). The relative textural and compositional
512 maturity of the sand fraction in the clay, as well as in the intervening quartz arenite, appears
513 to be compatible with a continental shallow marine depositional setting, probably in an
514 intracratonic basin. Assuming that the formation of authigenic clay by diagenesis or
515 shearing occurred soon after deposition, the sediments are c. 300–400 Ma younger than the
516 previously known Satakunta and Muhos graben formations (c. 1300 Ma) and c. 400 Ma
517 older than the Hailuoto and Taivalkoski formations (Fig. 2).

518 Other Tonian-Cryogenian isotope ages for sedimentary rocks that are related to faulting in
519 the Fennoscandian Shield have been dated in the Visingsö group, in the uppermost unit
520 (663 Ma) in Lake Vättern, Sweden, close to the Sveconorwegian front (Bonhomme and
521 Welin 1983), and in the Vadsø Group (825 ± 19 My) and Vestertana Group (668 ± 7 My)
522 in the Varanger peninsula, Norway, the northeastern margin of the Fennoscandian Shield
523 (Pringle, 1972; Sturt et al., 1975) (Figs 1 and 2). These are Rb–Sr ages and interpreted as
524 ages for diagenesis.

525

7. Conclusions

This study reports a unique fresh and unweathered authigenic clay from a tunnel site to record the timing of brittle faulting in southern Finland. Fig. 2 highlights an age compilation of the complex time constraints of the Fennoscandian basement including brittle fault, paleontological (microfossil), seismic and drilling data to constrain the new obtained clay isotope data.

A NNE-trending fracture opened in the Palaeoproterozoic basement in the Tonian period before c. 967 Ma. The age is documented by the 2–6 μm K–Ar illite age from the clay that filled the 30-cm-wide crevasse. The neocrystallization took place in diagenesis or reactivation of the fracture/fault after deposition. E–W-oriented extensional conditions prevailed locally, and the opening of the fracture is linked with the collapse of the Sveconorwegian orogeny in the west. Similar ages have been reported from fault gouges from Olkiluoto drill cores, and many of the brittle faults in the basement can probably be attributable to the orogen collapse. The similar geometry and shear sense indicators of other brittle faults may henceforth be related to this event.

The smaller illite crystals (<0.4 μm) in Myras clay with a K–Ar age of c. 809–697 Ma may record:

a) Reactivation of the fault. No known tectonic activity in the area has previously been documented, but continental break-up of the Rodinia supercontinent started at that time in the west and may have caused the reactivation and formation of new faults in the crust far from its proximal areas;

b) Less probable thermal overprint related to the Caledonian orogeny at ≥ 400 Ma. The previously studied Caledonian ages suggesting thermal effect in Finland have formed in much lower temperatures than required for illite neocrystallization. Clay Argon diffusion calculations indicate that diffusion might influence the <0.1 μm fraction, but is unlikely to impact on the coarser clay fractions (0.1–0.4 μm) within 800 Ma. Furthermore, the thick clay deposit is compact and has a low permeability for hydrothermal fluids.

The clay deposit and intervening quartz arenite are interpreted as being deposited in a shallow marine intracratonic basin. The age estimation of c. 967 Ma provides evidence for deposition within a time interval where sedimentary records from Fennoscandian shield are scarce, and related geochronological data are almost non-existent.

Acknowledgements

Andrew Todd and Mark Raven at CSIRO and Sari Lukkari, Mia Tiljander and Lassi Pakkanen in the Research Laboratory, GTK, are thanked for technical assistance during the study. Piri Harju of Pöyry, Finland, is thanked for providing the samples of clay material. Anneli Uutela, University of Helsinki, is thanked for the fossil analysis and Philip Stickler for drafting the Figs. 10 and 11. The Academy of Finland is acknowledged for partial support of this research (AK). We are grateful to the editor G. Zhao and reviewer G. Viola for their constructive and helpful reviews.

References

Alm, E., Sundblad, K., Huhma, H., 2005. Sm-Nd isotope determinations of low-temperature fluorite-calcite-galena mineralization in the margins of the Fennosciandian Shield: Report of activities carried out during 2004. Stockholm: Svensk Kärnbränslehantering. 58p

Aronson, J.L., Hower, L., 1976. Mechanism of burial metamorphism of agrillaceous sediments. 2. Radiogenic argon evidence. Geol. Soc. Amer. Bull. 87, 738-744.

Amantov, A., Hagenfeldt, S., Södeberg, P., 1995. The Mesoproterozoic to lower Palaeozoic sedimentary bedrock sequence in the northern Baltic proper, Åland Sea, Gulf of Finland and Lake Ladoga. Prace - Panstwowego Instytutu Geologicznego CXLIX, 19-25.

Bergman, L., 1982. Clastic dykes in the Åland Islands, SW Finland and their origin. Geol. Surv. Finland Bull. 317, 7-27.

Bingen, B., Nordgulen, Ø., Viola, G., 2008. A four-phase model for the Sveconorwegian orogeny, SW Scandinavia. Norw. J. Geol. 88, 430-72.

Bonhomme, M.G., Thuizat, R., Pinault, Y., Clauer, N., Wendling, R., Winkler, R., 1975. Méthode de datation potassium-argon. In: Appareillage et Technique, Strasbourg, 53pp.

Bonhomme, M.G, Welin, E., 1983. Rb-Sr and K-Ar isotopic data on shale and siltstone from the Visingö group, Lake Vättern basin, Sweden. Geol. Fören. Stock. För. 105, 363–366.

Clauer, N., Chaudhuri, S., 1995. Clays and Crustal Cycles, Springer, Heidelberg, Germany.

589 Choo, C.O., Chang, T.W., 2000. Characteristics of clay minerals in gouges of the Dongrae
590 fault, Southeastern Korea, and implications for fault activity. Clays Clay Miner. 48, 204–
591 212.

592 Dalrymple, G.B., Lanphere, M.A., 1969. Potassium-argon dating: principles, techniques
593 and applications to geochronology. San Francisco: W.H. Freeman.

594 Duvall, A.R., Clark, M.K., van der Pluijm, B.A., Chuanyou, L., 2011. Direct dating of
595 Eocene reverse faulting in northeastern Tibet using Ar-dating of fault clays and low-
596 temperature thermochronometry. Earth Planet. Sci. Lett. 304, 520–526.

597 Elminen, T., Vaarma, M., Wennerström, M., Pajunen, M., Wasenius, P., 2007. Savion
598 rautatietunnelin rakennegeologinen kartoitus. Geological Survey of Finland, archive report
599 K21.42/2007/48. 29 p. (in Finnish)

600 Elminen, T., Airo, M.-L., Niemelä, R., Pajunen, M, Vaarma, M., Wasenius,
601 P.,Wennerström, M., 2008. Fault structures in the Helsinki area, Southern Finland. In:
602 Pajunen, M. (Ed.), Tectonic evolution of the Svecofennian crust in southern Finland - a
603 basis for characterizing bedrock technical properties. Geol. Surv. Finland, Spec. Paper 47,
604 185–213.

605 Elo, S., Kuivasaari, T., Lehtinen, M. Sarapää, O., Uutela, A., 1993. Iso-Naakkima, a
606 circular structure filled with Neoptoterozoic sediments, Pieksämäki, southeastern Finland.
607 Bull. Geol. Soc. Finland 65, 3–30.

608 Gradstein, F., Ogg, J., Smith, A., 2004. A Geologic Time Scale 2004. Cambridge
609 University Press, Cambridge.

610 Haines, S.H., van der Pluijm, B.A., 2008. Clay quantification and Ar-Ar dating of synthetic
611 and natural gouge – Application to the Miocene Sierra Mazatán detachment fault, Sonora,
612 Mexico. J. Struct.Geol. 30, 525–538.

613 Hagenfeldt, S.E., 1995. Erratics and Proterozoic-Lower Palaeozoic submarine sequences
614 between Åland and mainland Sweden. Geological Survey of Sweden, Research papers,
615 SGU series Ca 84, 1-35 p.
616 Hamilton, P.J., Kelley, S., Fallick, A.E., 1989. K-Ar Dating of illite in hydrocarbon
617 reservoirs. Clays Clay Minerals 24, p. 215-231.

618 Heeremans, M., Wijbrans, J., 1999. Late Proterozoic tectonic events in southern Finland,
619 constrained by 40Ar/39Ar incremental heating and single spot fusion experiments on K-
620 feldspars. Terra Nova 11, 216-222.

621 Hess, J.C., Lippolt, H.J., 1994. Compilation of K/Ar measurements on HD-B1 standard
622 biotite; 1994 status report. In: G. S. Odin (Ed.), Phanerozoic Time Scale. Paris: Bulletin de
623 Liaison et d'information, IUGS Subcommission, Geochronology. pp. 19–23

624 Hetzel, R., Zwingmann, H., Mulch, A., Gessner, K., Akal, C., Hampel, A., Güngör, T.,
625 Petschick, R., Mikes, T., Wedin, F., 2013. Spatiotemporal evolution of brittle normal
626 faulting and fluid infiltration in detachment fault systems: A case study from the Menderes
627 Massif, western Turkey. Tectonics 32, 364–376.

628 Huon, S., Cornée, J.J., Piqué, A., Rais, N., Clauer, N., Liewig, N., Zayane, R., 1993. Mise
629 en évidence au Maroc d'événements thermiques d'âge triascico-liasique liés à l'ouverture de
630 l'Atlantique. Bull. Soc. Géol. Fr. 164, 165–176.

631 Hyyppä, J., Pekkala, Y., 1987. Tutkimustyöselostus Taivalkosken kunnassa valtausalueilla
632 Saarijärvi 1-3 (kaiv.rek.nro 3156/1-3) suoritetuista savikivitutkimuksista. Geological
633 Survey of Finland, Claim report M 06/3533/-87/1/89. 39 p

634 Kohonen, J., Rämö, O.T., 2005. Sedimentary rocks, diabases, and late cratonic evolution.
635 In: Lehtinen, M., Nurmi, P., Rämö, O.T. (Eds.), Precambrian Geology of Finland – Key to
636 the Evolution of the Fennoscandian Shield. Developments in Precambrian Geology 14,
637 563–603.

638 Koistinen, T., Klein, V., Koppelmaa, H., Korsman, K., Lahtinen, R., Nironen, M., Puura,
639 V., Saltykova, T., Tikhomirov, S., Yanovskiy, A., 1996. Paleoproterozoic Svecofennian
640 orogenic belt in the surroundings of the Gulf of Finland In: Koistinen T., (Ed.), Explanation
641 to the Map of Precambrian basement of the Gulf of Finland and surrounding area 1:1
642 million. Geol. Surv. Finland, Spec. Paper 21, 21–57.

643 Kralik, M., Klima, K., Riedmüller, G., 1987. Dating fault gouges. Nature 327, 315–317.

644 Kralik, M., Clauer, N. Holnsteiner, R. Huemer, H., Kappel, F., 1992. Recurrent fault
645 activity in the Grimsel Teat site (GTS, Switzerland): revealed by Rb-Sr, K-Ar and tritium
646 isotope techniques. J. Geol. Soc. London 149, 293–301.

647 Kumpulainen, R., Nystuen, J.P., 1985. Late Proterozoic basin evolution and sedimentation
648 in the westernmost part of Baltoscandia. In: Gee, D.G.,Sturt, B.A., (Eds.), The Caledonide
649 Orogen--Scandinavia and Related Area. Wiley, Chichester, pp. 213–232.

650 Laitakari, I., Rämö, T., Suominen, V., Niin, M., Stepanov, K., Amantov, A., 1996.
651 Subjotnian: Rapakivi granites and related rocks in the surroundings of the Gulf of Finland.

652 In: Koistinen, T., (Ed.), Explanation to the Map of Precambrian basement of the Gulf of
653 Finland and surrounding area 1:1 million. Geol. Surv. Finland, Spec. Paper 21, 59–97.

654 Larson, S., Åke, Tullborg, E.-L., Cederbom, C., Stiberg, J.-P., 1999. Sveconorwegian and
655 Caledonian foreland basins in the Baltic Shield revealed by fission-track
656 thermochronology. Terra Nova 11, 210-215.

657 Lehtovaara, J.J., 1995. Pre-Quaternary rocks of the Kilpisjärvi and Halti map-sheet areas.
658 Geological map of Finland 1:100 000. Explanation to the maps of Pre-Quaternary rocks.
659 Sheets 1823 and 1842. Geol. Surv. Finland, 64 p. (in Finnish with an English summary)

660 Liewig, N., Clauer, N., Sommer, F., 1987. Rb-Sr and K-Ar dating of clay diagenesis in
661 Jurassic sandstone oil-reservoir, North-Sea. AAPG Bull. 71, 1467–1474.

662 Lyons, J.B., Snellenberg, J., 1971. Dating faults: Geol. Soc. Am. Bull. 82, 1749–1752.

663 Mattila, J. and Viola, G., 2014. New constraints on 1.7 Gyr of brittle tectonic evolution in
664 southwestern Finland derived from a structural study at the site of a potential nuclear waste
665 repository (Olkiluoto Island). J. Struct. Geol. 67, 50–74.

666 Mertanen, S., Airo, M., Elminen, T., Niemelä, R., Pajunen, M., Wasenius, P.,
667 Wennerström, M., 2008. Paleomagnetic evidence for Mesoproterozoic - Paleozoic
668 reactivation of the Paleoproterozoic crust in southern Finland. In: Pajunen, M., (Ed.),
669 Tectonic evolution of the Svecofennian crust in southern Finland - a basis for
670 characterizing bedrock technical properties. Espoo: Geol. Surv. Finland, Spec. Paper 47,
671 215–252.

672 Meunier, A., Velde, B., Zalba, P., 2004. Illite K–Ar dating and crystal growth processes in
673 diagenetic environments: a critical review. Terra Nova, 16, 296–304.

674 Mulch, A., Cosca, M. A., Andresen, A and Fiebiga,J., 2005. Time scales of deformation
675 and exhumation in extensional detachment systems determined by high-spatial resolution in
676 situ UV-laser 40Ar/39Ar dating. Earth Planet. Sci. Lett. 233, 375– 390

677 Murrel, G., 2003. The long -term thermal evolution of Central Fennoscandia. Vrije
678 Universiteit, The Netherlands. 219 p. (dissertation)

679 Odin, G.S., 1975. De glauconarium constitutione, aetateque: Ph.D. thesis, University of
680 Paris-Sud, 280 p.

681 Patchett, P.J., 1978. Rb/Sr ages of Precambrian dolerites and syenites in South and Central
682 Sweden. Geological Survey of Sweden SGU C747, 1-63.

683 Pajunen, M., Airo M.-L., Elminen T., Mänttäri I., Niemelä R., Vaarma M., Wasenius P.,
684 Wennerström, M., 2008. Tectonic evolution of the Svecofennian crust in southern Finland.
685 In: Pajunen, M., (Ed.), Tectonic evolution of the Svecofennian crust in southern Finland - a
686 basis for characterizing bedrock technical properties. Geol. Surv. Finland, Spec. Paper 47,
687 15–184.

688 Pesonen, L.J., Lehtinen, M., Tuukki, P., Abels, A., 1998. The Lake Saarijärvi - a new
689 meteorite impact structure in northern Finland (PDF). Lunar and Planetary Science 29,
690 1262.

691 Pleuger, J., Mancktelow, N., Zwingmann, H., Manser, M., 2012. K-Ar dating of
692 synkinematic clay gouges from Neoalpine faults of the Central, Western and Eastern Alps.
693 Tectonophysics 550-553, 1-16, doi:10.1016/j.tecto.2012.05.001.

694 Pokki, J., 2006. Report on the Database of Post-Svecofennian Sedimentary Rocks in
695 Finland. Geological Survey of Finland, archive report K 21.42/2006/4. 21p.

696 Pokki, J., Kohonen, J., Lahtinen, R., Rämö, T., Andersen, T., 2013. Petrology and
697 provenance of the Mesoproterozoic Satakunta Formation, SW Finland. Report of
698 Investigation 204. Geological Survey of Finland.

699 Porrenga, D.H., 1967. Glauconite and chamosite as depth indicators in the marine
700 environment. Mar. Geol. 5, 495–501.

701 Pringle, I. R., 1972. Rb-Sr age determinations on shales associated with the Varanger Ice
702 Age. Geol. Mag. 109, 465-472.

703 Redfield, T.F., 2010. On apatite fission track dating and the Tertiary evolution of West
704 Greenland topography: J. Geol. Soc. London 167, 261–271, doi: 10.1144/0016-76492009-
705 036.

706 Roberts, D. and Siedlecka, A., 2002. Timanian orogenic deformation along the northeastern
707 margin of Baltica, Northwest Russia and Northeast Norway, and Avalonian–Cadomian
708 connections. Tectonophysics 352, 169–184.

709 Sandström, B., Tullborg, E.-L., Larson, S. Å., Page, L., 2009. Brittle tectonothermal
710 evolution in the Forsmark area, central Fennoscandian Shield, recorded by paragenesis,

711 orientation and 40Ar/39Ar geochronology of fracture minerals. Tectonophysics 478, 158-
712 174.

713 Sasseville, C., Tremblay, A., Clauer, N., Liewig, N., 2008. K-Ar age constraints on the
714 evolution of polydeformed fold-thrust belts: The case of the Northern Appalachians
715 (southern Quebec): J. Geodyn. 45, 99–119.

716 Simonen, A., 1980. The Precambrian in Finland. Geol. Surv. Finland Bull. 304, 58 p.

717 Solum, J. G., van der Pluijm, B. A., Peacor, D. R., 2005. Neocrystallization, fabrics and age
718 of clay minerals from an exposure of the Moab Fault. J. Struct. Geology 27, 1563–1576.

719 Steiger, R.H., Jäger, E., 1977. Subcommission on geochronology: convention on the use of
720 decay constants in geo- and cosmochronology. Earth Planet. Sci. Lett. 36, 359–362.

721 Sturt, B.A., Pringle, I.R., Roberts, D., 1975. Caledonian Nappe Sequence of Finnmark,
722 Northern Norway, and the Timing of Orogenic Deformation and Metamorphism. Geol.
723 Soc. Am. Bull. 86, 710-718.

724 Suominen, V., 1991. The chronostratigraphy of southwestern Finland with special reference
725 to Postjotnian and Subjotnian diabases. Geol. Surv. Finland Bull. 356. 100 p.

726 Söderberg, P., 1993. Seismic stratigraphy, tectonics and gas migration in the Åland Sea,
727 northern Baltic proper. Stockholm Contributions in Geology 43, 1-67.

728 Thorslund, P., Axberg, S., 1979. Geology of the southern Bothnian Sea; Part I. Bull. Geol.
729 Inst. Univ. Uppsala, New Series 8, 35-62.

730 Torgersen, E., Viola G., Zwingmann, H., Harris, C., 2014. Structural and temporal
731 evolution of a reactivated brittle–ductile fault – Part II: Timing of fault initiation and
732 reactivation by K–Ar dating of synkinematic illite/muscovite. Earth Planet. Sci. Lett. 407,
733 221–233.

734 Tullborg, E-L., Larson, S.Å., Björklund, L., Samuelsson, L., Stigh, J., 1995. Thermal
735 evidence of Caledonide foreland, molasse sedimentation in Fennoscandia. Swedish Nuclear
736 Fuel and Waste Managements, SKB TR 95-18.

737 Tynni, R., 1978. Lower Cambrian fossils and acritarchs in the sedimentary rocks of
738 Söderfjärden, Western Finland. Geol. Surv. Finland Bull. 297, 39–81.

739 Tynni, R., 1982. On Paleozoic microfossils in clastic dykes in the Åland Islands and in the
740 core samples of Lumparn. Geol. Surv. Finland Bull. 317, 35–114.

741 Tynni, R., Donner, J., 1980. A microfossil and sedimentation study of the Late Precambrian
742 formation of Hailuoto, Finland. Geol. Surv. Finland Bull. 311, 1-27.

743 Tynni, R., Hokkanen, K., 1982. Traces of crawling by annelids in Lauhanvuori sandstone.
744 Geologi 7, 129-134. (in Finnish with an English summary)

745 Tynni, R., Uutela, A., 1984. Microfossils from the Precambrian Muhos formation in
746 Western Finland. Geol. Surv. Finland Bull. 330, 38 p.

747 Tynni, R., Uutela, A., 1985. Myöhäisprekambrinen ajoitus Taivalkosken savikivelle
748 mikrofossiilien perusteella. Late Precambrian shale formation of Taivalkoski in northern
749 Finland. Geologi 37, 61–65. (in Finnish with English summary)

Törnroos, R., 1984. Petrography, mineral chemistry and petrochemistry of granite porphyry dykes from Sibbo, southern Finland. Geol. Surv. Finland Bull. 326, 1-43.

Uutela, A., 1990. Proterozoic microfossils from the sedimentary rocks of the Lappajärvi impact crater. Bull. Geol. Soc. Finland 62, 115-120.

Uutela, A., 2001. Proterozoic and early Palaeozoic microfossils in the Karikkoselkä impact crater, central Finland. Bull. Geol. Soc. Finland 73, 75-85.

Vaasjoki, M., 1977. Rapakivi granites and other postorogenic rocks in Finland: their age and lead isotopic composition of certain associated galena mineralizations. Geol. Surv. Finland Bull. 294, 1-64.

Vaasjoki, M., Appelqvist, H., Kinnunen, K.A. 2002. Paleozoic remobilisation and enrichment of Proterozoic uranium mineralisation in the East-Uusimaa area, Finland. In: Lithosphere 2002: Second Symposium on the Structure, Composition and Evolution of the Lithosphere in Finland, Espoo, Otaniemi, November 12-13, 2002: programme and extended abstracts. Institute of Seismology. University of Helsinki. Report S-42. Helsinki: Institute of Seismology 139.

Vaasjoki, M., Korsman, K., Koistinen, T., 2005. Overview. In: Lehtinen, M., Nurmi, P., Rämö, O.,T., (Eds), Precambrian geology of Finland Key to the evolution of the Fennoscandian shield. Elsevier, 1-16.

Van der Pluijm, B.A., Hall, C.M., Vrolijk, P.J., Pevear, D.R., Covey, M.C., 2001. The dating of shallow faults in the Earth's crust. Nature 412, 172–175.

770 Viola, G., Zwingmann, H., Mattila, J., Käpyaho, A., 2013. K-Ar illite age constraints on the
771 Proterozoic formation and reactivation history of a brittle fault in Fennoscandia. Terra
772 Nova 25, 236–244.

773 Viola, G., Mattila, J., Zwingmann, H., Todd, A., 2011. Structural and K/Ar illite
774 geochronological constraints on the brittle deformation history of the Olkiluoto region,
775 Southwest Finland. Posiva working report 2011-37, 170 p. www.posiva.fi.

776 Viola, G., Scheiber, T., Fredin, O., Zwingmann, H., Margreth, A., Knies, J., 2016.
777 Deconvoluting complex structural histories archived in brittle fault zones. Nat. Commun.
778 7:13448 | DOI: 10.1038/ncomms13448.

779 Vrolijk, P., van der Pluijm, B.A., 1999. Clay gouge. J. Struct. Geol. 21, 1039–1048.

780 Väisänen, M., Skyttä, P., 2007. Late Svecofennian shear zones in southwestern Finland.
781 GFF 129, 55–64.

782 Wannäs, K.O., Flodén, T., 1994. Tectonic framework of the Hanö Bay area, southern Baltic
783 Sea. Svensk Kärnbränslehantering AB, Technical Report 94-09, 40 p.

784 Winterhalter, B., 1982. The bedrock geology of Lumparn Bay, Åland. Geol. Surv. Finland
785 Bull. 317, 115-130.

786 Wijbrans, J.R., McDougall, I., 1986. 40Ar/39Ar dating of white micas from an Alpine
787 highpressure metamorphic belt on Naxos (Greece): The resetting of the argon isotopic
788 system. Contrib. Mineral. Petrol. 93, 187-194.

789 Winterhalter, B., Flodén, T., Ignatius, H., Axberg, S., Niemistö, L., 1981. Geology of the
790 Baltic Sea. In: Voipio, A., (Ed.), The Baltic Sea. Elsevier Oceanography Series 30.
791 Amsterdam: Elsevier, pp. 1–121.

792 Yamasaki, S., Zwingmann, H., Yamada, K., Tagami, T., Umeda, K., 2013. Constraining
793 the timing of brittle deformation and faulting in the Toki granite, central Japan. Chem.
794 Geol. 351, 168–174.

795 Zwingmann, H., Han, R., Ree, J.H., 2011. Cretaceous reactivation of the Deokpori Thrust,
796 Taebaeksan Basin, South Korea, constrained by K-Ar dating of clayey fault gouge.
797 Tectonics 30, doi:10.1029/2010TC002829.

798 Zwingmann, H., Mancktelow, N., 2004. Timing of Alpine fault gouges. Earth Planet. Sci.
799 Lett. 223, 415–425.

800 Zwingmann, H., Mancktelow, N., Antognini, M., Lucchini, R., 2010a. Dating of shallow
801 faults: New constraints from the AlpTransit tunnel site (Switzerland). Geology 38, 487–
802 490.

803 Zwingmann, H., Yamada, K., Tagami, T., 2010b. Timing of brittle faulting within the
804 Nojima fault zone, Japan. Chem. Geol. 275, 176–185;
805 doi:10.1016/j.chemgeo.2010.05.006.

806

Highlights

- Investigation of fresh clay originating from a tunnel fracture site in Finland.
- The clay was deposited in a shallow marine basin in Paleoproterozoic bedrock.
- K-Ar dating of illite documents neocrystallization at c. 967 Ma after brittle faulting.
- Reactivation of the fracture occurred at c. 697 Ma.
- Brittle deformations are linked to Sveconorwegian orogeny and continental break-up.

807 **Figure captions**

808

809 Figure 1. (A) A schematic geological map of the Fennoscandian shield and locations of the
810 Myras study site and sedimentary rock formations in Finland and Fennoscandia and other
811 locations mentioned in the text. (B) A bedrock map of southwestern Finland. The yellow
812 circle (MYR) indicates the Myras sampling point. Orange squares denote Olkiluoto (OLK),
813 the uraninite dating point (LAK), and a fluorite vein (LOV). Green diamonds indicate
814 palaeomagnetic measurements; (PM) Porkkala-Mäntsälä fault; small blue dots arenite dyke
815 locations and (S) Satakunta Graben.

816 Figure 2. Age compilation summary figure with paleontological (microfossil), seismic,
817 drilling, dated brittle fault and clay isotope data of Fennoscandia for the Mesoproterozoic
818 and Neoproterozoic. For Finland all data from 1400 Ma to 542 Ma are presented and from
819 Sweden and Norway essential data based on Suominen (1991), Winterhalter et al. (1981),
820 Thorslund and Axberg (1979), Simonen (1980), Tynni and Uutela (1984, 1985), Tynni and
821 Donner (1980), Wannäs and Flodén (1994), Söderberg (1993), Hagenfeldt (1995),
822 Amantov et al. (1995), Bonhomme and Welin (1983), Sturt et al. (1975), Tynni (1982),
823 Patchett (1978), Tynni and Hokkanen (1982), Lehtovaara (1995), Elo et al. (1993),
824 Bergman (1982), Winterhalter (1982), Uutela (1990, 2001), Tynni (1978), Heeremans and
825 Wijbrans (1999), Sandström et al. (2009), Torgersen et al. (2014), Mulch et al. (2005),
826 Viola et al. (2013). Porkkala-M=Porkkala- Mäntsälä shear zone and fault, Porsgrunn-
827 K=Porsgrunn-Kristiansand shear zone.

828 Figure 3. (A) A sketch of 220 m tunnel floor showing the Myras clay, the fault structures,
829 the drill cores and the sampling points. (B) A sketch of the clay-filled fracture with the
830 tunnel cross section, drill cores and drill core sections with sedimentary rocks. Not to scale.

831 Figure 4. (A) K–Ar clay samples. (B) The sampling site at Myras with white arenite, the
832 clay deposit and clay/gouge exposed on the tunnel wall. SL = slickenline. The red material
833 is quarrying dirt.

834 Figure 5. Close-ups from drill cores. (A) Bedding structure in quartz sand. (B) Sheared clay
835 with quartz grains.

836 Figure 6. Quartz grains decanted from the clay sample.

837 Figure 7. Petrographic SEM and TEM images of authigenic illite with representative EDS
838 spectra. (A, B) images of the clay surface of sample TU4-38040 by SEM. (C, D) TEM
839 images of sample 1710 <0.1 μm fraction. Typical illite morphology confirmed by EDS is
840 indicated by circles.

841 Figure 8. Thin section images of quartz arenite. (A) Well rounded quartz grains and a
842 silicified clay chip in the lower part. (B) The arrow points to intersitial glauconite. The
843 trace is left by the EPMA beam. (C) BSE image from the clay chip in Figure A. Most of the
844 material is silicified (Q), some illite (I) is left. (D) Microcataclasite in the arenite.

845 Figure 9. A K–Ar age plot; ages are summarized within the geological and
846 geochronological context of the study area.

847 Figure 10. Brittle fault succession in Myras area with assumed stress fields. (A) Ductile
848 NE-trending steep shear zones that later have developed to semi-brittle and brittle faults.

849 PM Porkkala-Mäntsälä shear/fault zone. (B) Brittle faulting following ca. 1650 Ma rapakivi
850 magmatism. B indicates Bodom rapakivi granite, D diabase dykes, P granite porphyry
851 dykes. NW-SE normal faults and dextral stikre-slip along NE-SW faults. (C) N-S oriented
852 vertical sinistral strike-slip faults crosscutting faults in figure B. (D) Myras fracture (M) in
853 an exaggerated scale. The stress field for NNE-trending fracture differs from that of the
854 other fault structures.

855 Figure 11. Summary of the interpretation of the obtained illite ages in the geological
856 framework of the study area. Mesoproterozoic magmatic events and known stress tensors in
857 Southern Finland are indicated. Myras fracture development is linked to Sveconorwegian
858 collapse and continental break-up in the west.

859 Figure 12. Clay argon diffusion plots temperature range 150 to 350 °C versus grainsize in
860 µm. (A) 0.1 µm, (B) 0.4 µm, C 2 µm, (D) 6 µm listing temperature legend. (E) 100 °C
861 overprint of grain sizes from 0.05, 0.1, 0.2, 2 and 6 µm over a 100 Ma timescale, (F) 150
862 °C overprint of grain sizes from 0.05, 0.1, 0.2, 2 and 6 µm over a 100 Ma timescale.

863 **Tables**

871

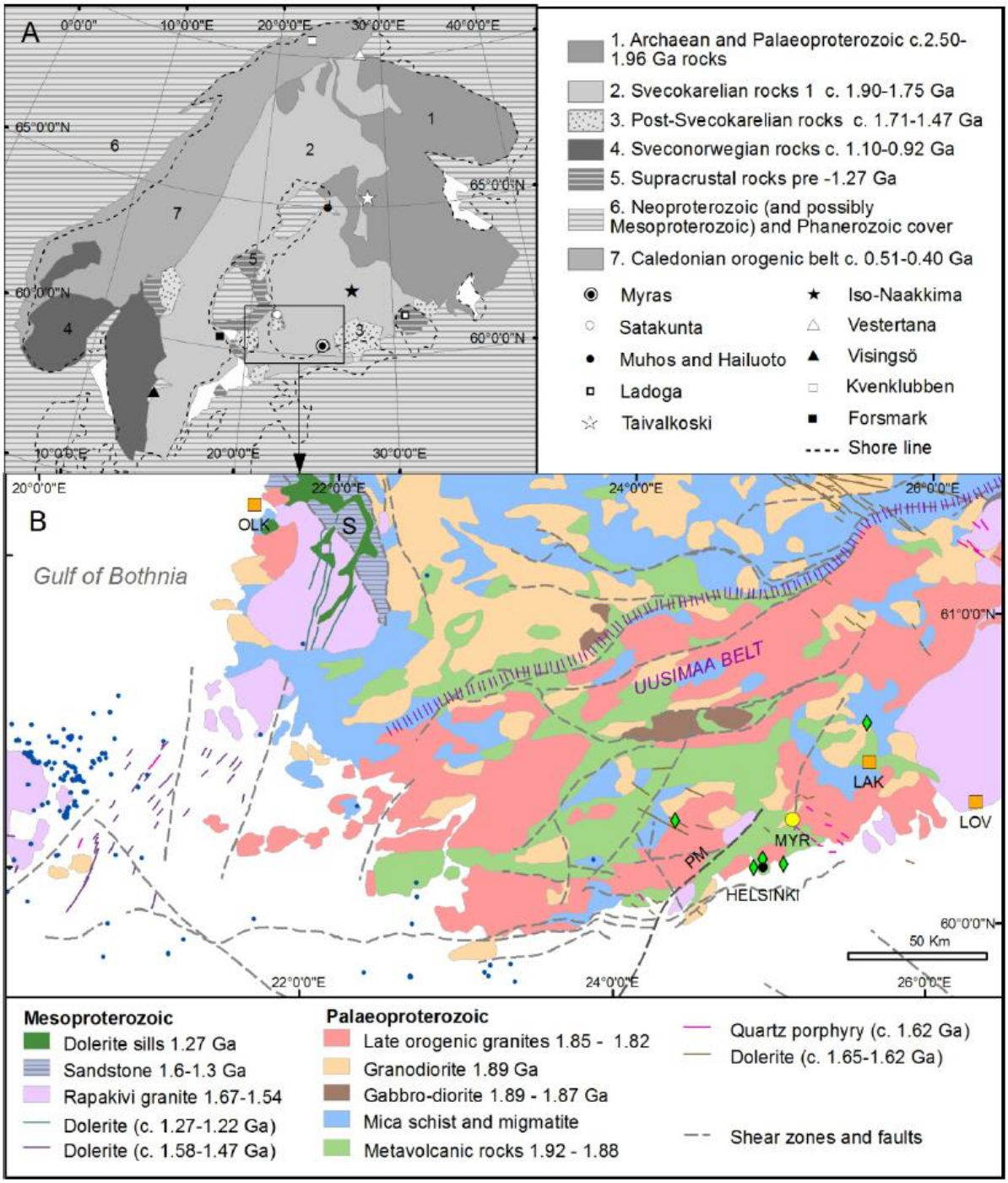
A
0°0'0"
10°0'0"E
20°0'0"E
30°0'0"E
40°0'0"E
65°0'0"N
60°0'0"N
1
2
3
4
5
6
7
1. Archaean and Palaeoproterozoic c.2.50-1.96 Ga rocks
2. Svecokarelian rocks 1 c. 1.90-1.75 Ga
3. Post-Svecokarelian rocks c. 1.71-1.47 Ga
4. Sveconorwegian rocks c. 1.10-0.92 Ga
5. Supracrustal rocks pre -1.27 Ga
6. Neoproterozoic (and possibly Mesoproterozoic) and Phanerozoic cover
7. Caledonian orogenic belt c. 0.51-0.40 Ga
Myras
Satakunta
Muhos and Hailuoto
Ladoga
Taivalkoski
Iso-Naakkima
Vestertana
Visingsö
Kvenklubben
Forsmark
Shore line
B
20°0'0"E
22°0'0"E
24°0'0"E
26°0'0"E
OLK
S
Gulf of Bothnia
61°0'0"N
UUSIMAA BELT
LAK
LOV
MYR
PM
HELSINKI
60°0'0"N
50 Km
Mesoproterozoic
Dolerite sills 1.27 Ga
Sandstone 1.6-1.3 Ga
Rapakivi granite 1.67-1.54
Dolerite (c. 1.27-1.22 Ga)
Dolerite (c. 1.58-1.47 Ga)
Palaeoproterozoic
Late orogenic granites 1.85 - 1.82
Granodiorite 1.89 Ga
Gabbro-diorite 1.89 - 1.87 Ga
Mica schist and migmatite
Metavolcanic rocks 1.92 - 1.88
Quartz porphyry (c. 1.62 Ga)
Dolerite (c. 1.65-1.62 Ga)
Shear zones and faults

Fig. 1

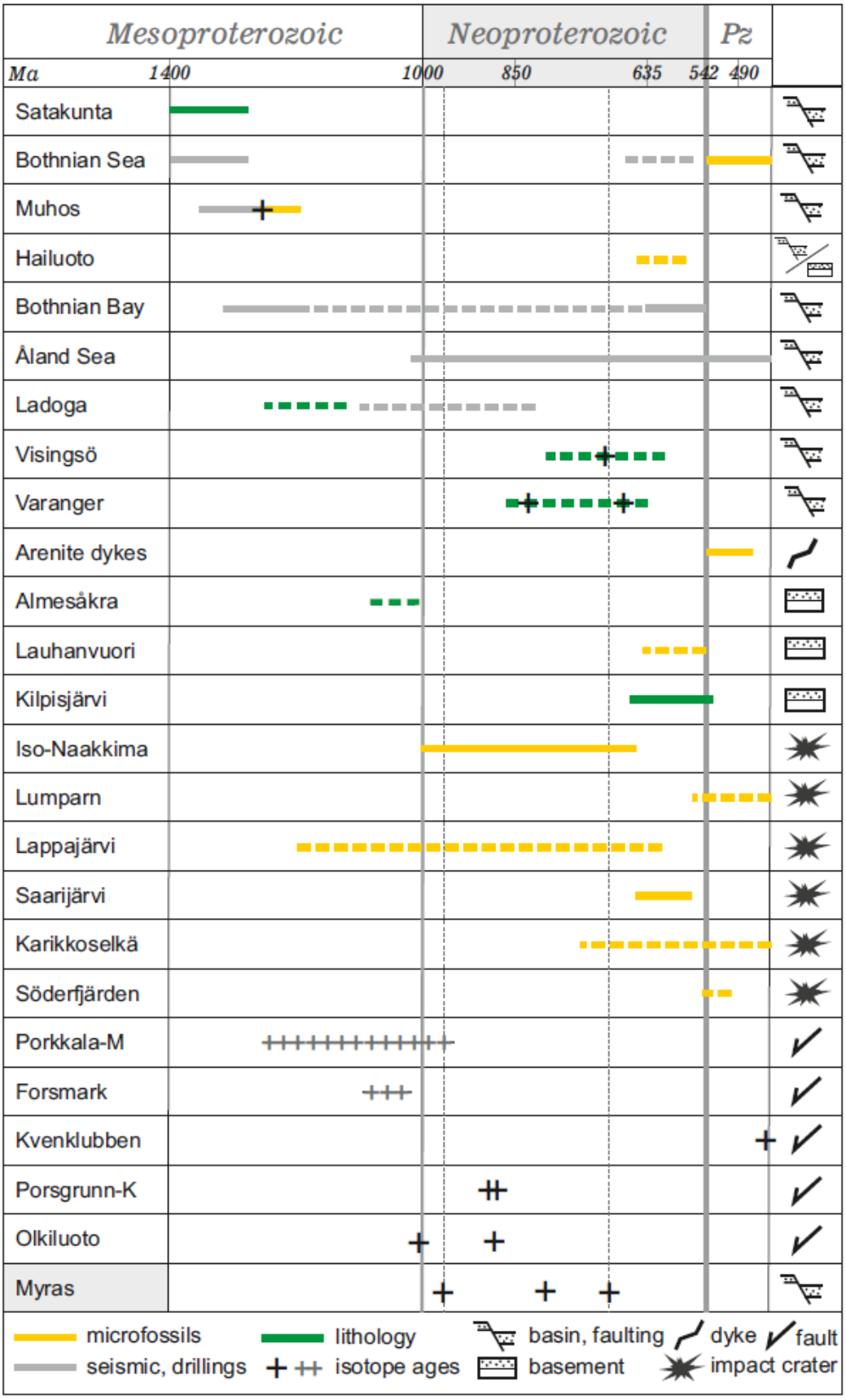
Mesoproterozoic
Neoproterozoic
Pz
Ma
1400
1000
850
635
542
490
Satakunta
Bothnian Sea
Muhos
Hailuoto
Bothnian Bay
Åland Sea
Ladoga
Visingsö
Varanger
Arenite dykes
Almesåkra
Lauhanvuori
Kilpisjärvi
Iso-Naakkima
Lumparn
Lappajärvi
Saarijärvi
Karikkoselkä
Söderfjärden
Porkkala-M
Forsmark
Kvenklubben
Porsgrunn-K
Olkiluoto
Myras
microfossils
seismic, drillings
lithology
isotope ages
basin, faulting
basement
dyke
impact crater
fault

Fig. 2

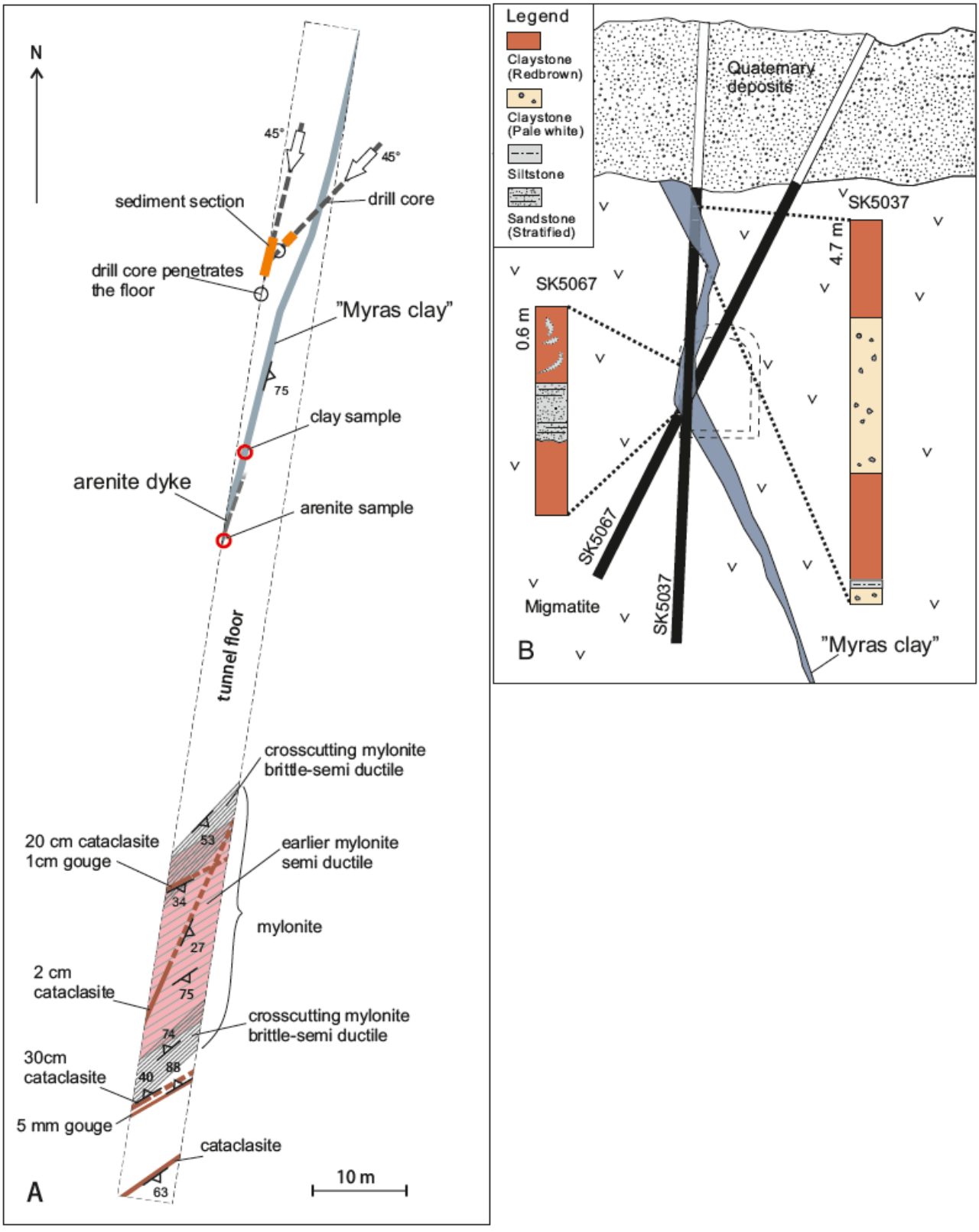
N
45°
45°
sediment section
drill core
drill core penetrates the floor
"Myras clay"
75
clay sample
arenite dyke
arenite sample
tunnel floor
crosscutting mylonite brittle-semi ductile
20 cm cataclasite
1cm gouge
53
earlier mylonite semi ductile
34
27
mylonite
2 cm cataclasite
75
74
crosscutting mylonite brittle-semi ductile
30cm cataclasite
40
88
5 mm gouge
cataclasite
63
10 m
A
Legend
Claystone (Redbrown)
Claystone (Pale white)
Siltstone
Sandstone (Stratified)
Quaternary deposits
SK5037
4.7 m
SK5067
0.6 m
SK5067
SK5037
Migmatite
"Myras clay"
B

Fig. 3

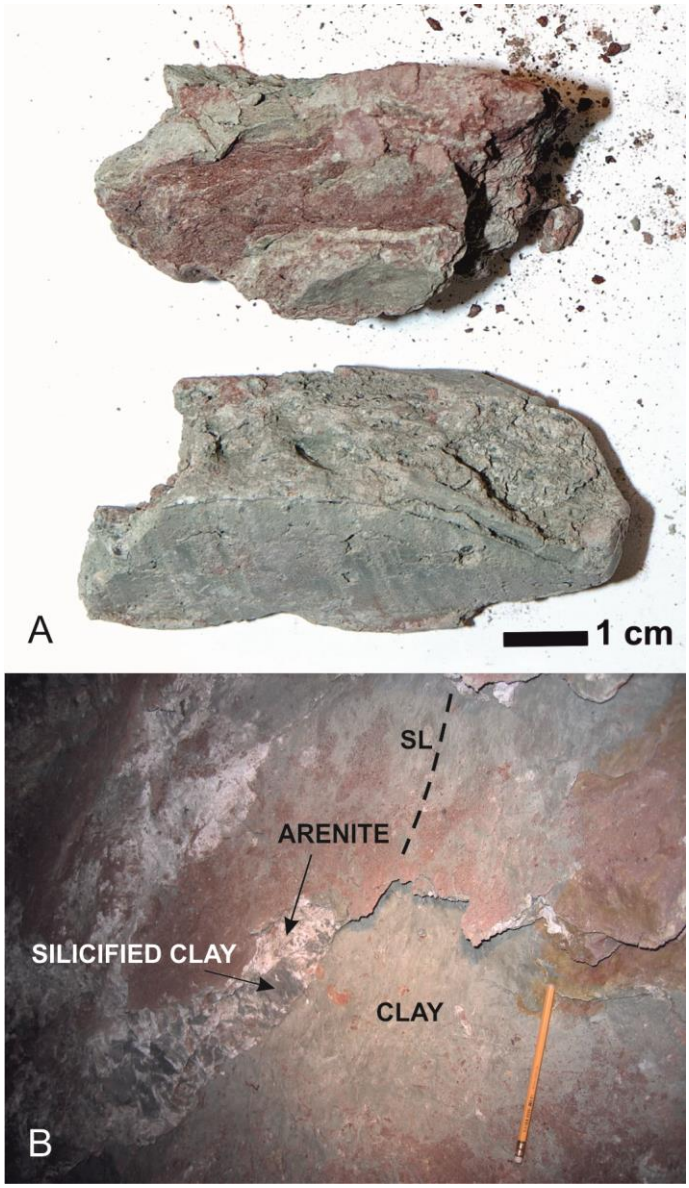

Fig. 4

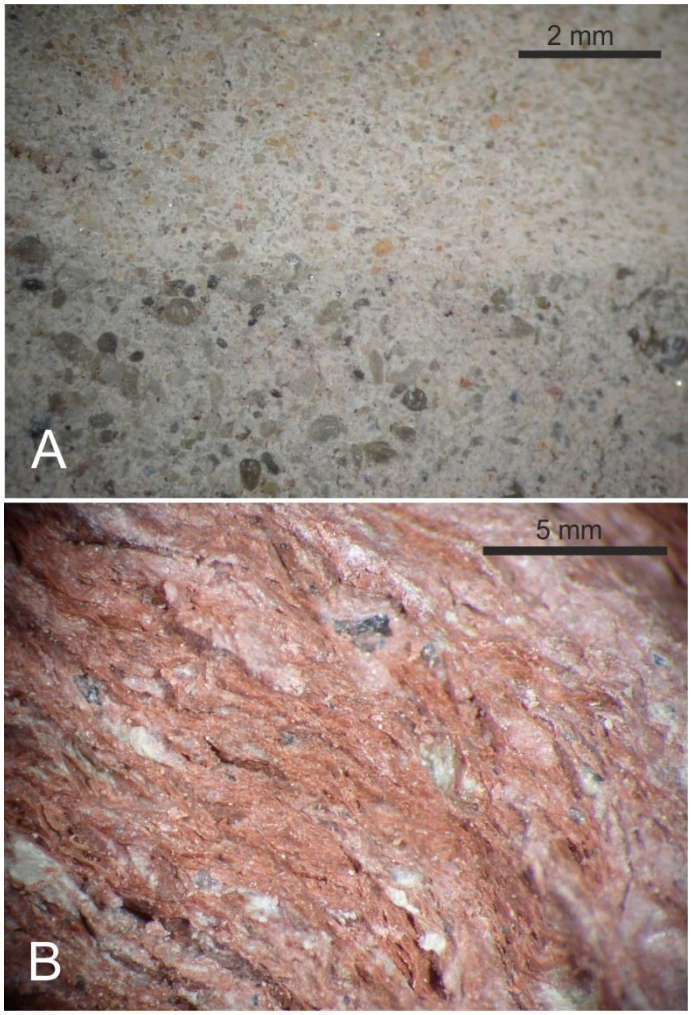

Fig. 5

Fig. 6

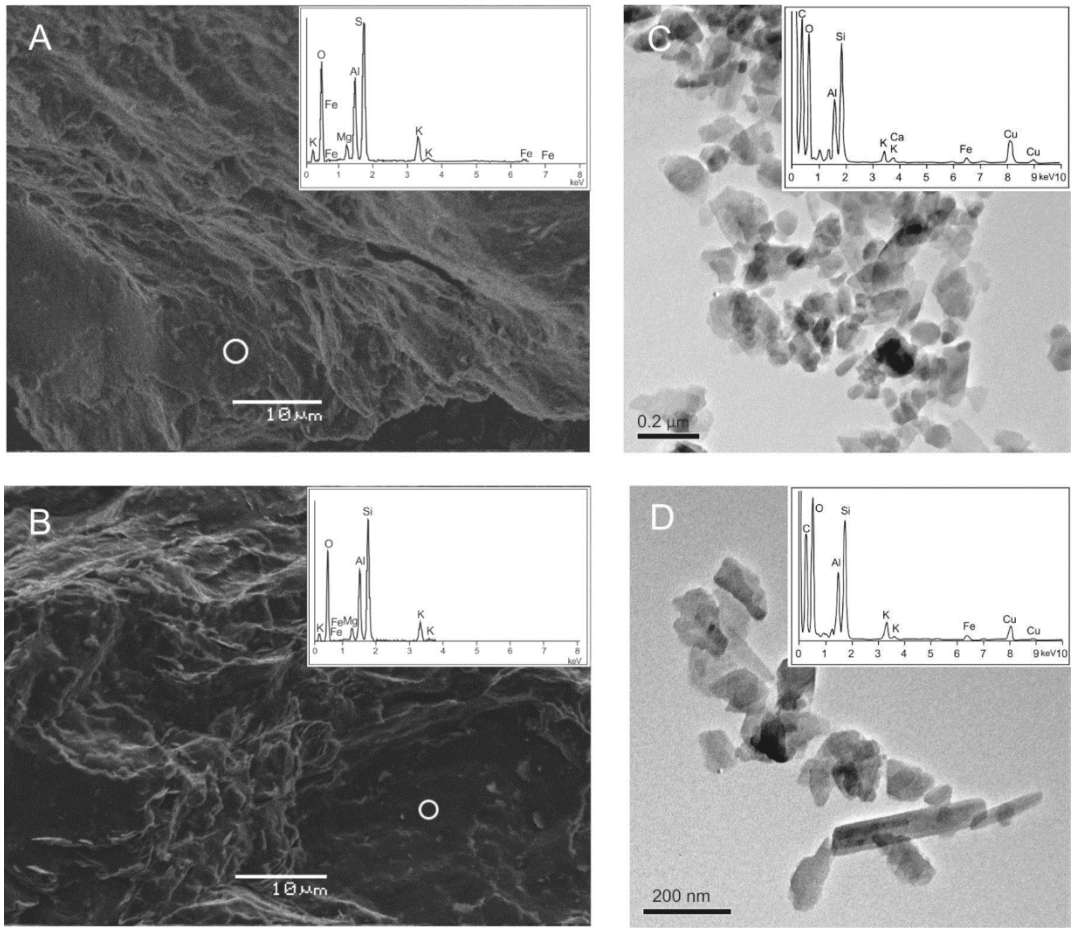
A
O
Si
Al
Fe
Mg
K
Fe
Fe
10 µm
B
O
Si
Al
K
Fe
Mg
K
10 µm
C
C
O
Si
Al
K
Ca
K
Fe
Cu
Cu
0.2 µm
D
C
O
Si
Al
K
K
Fe
Cu
Cu
200 nm

Fig. 7

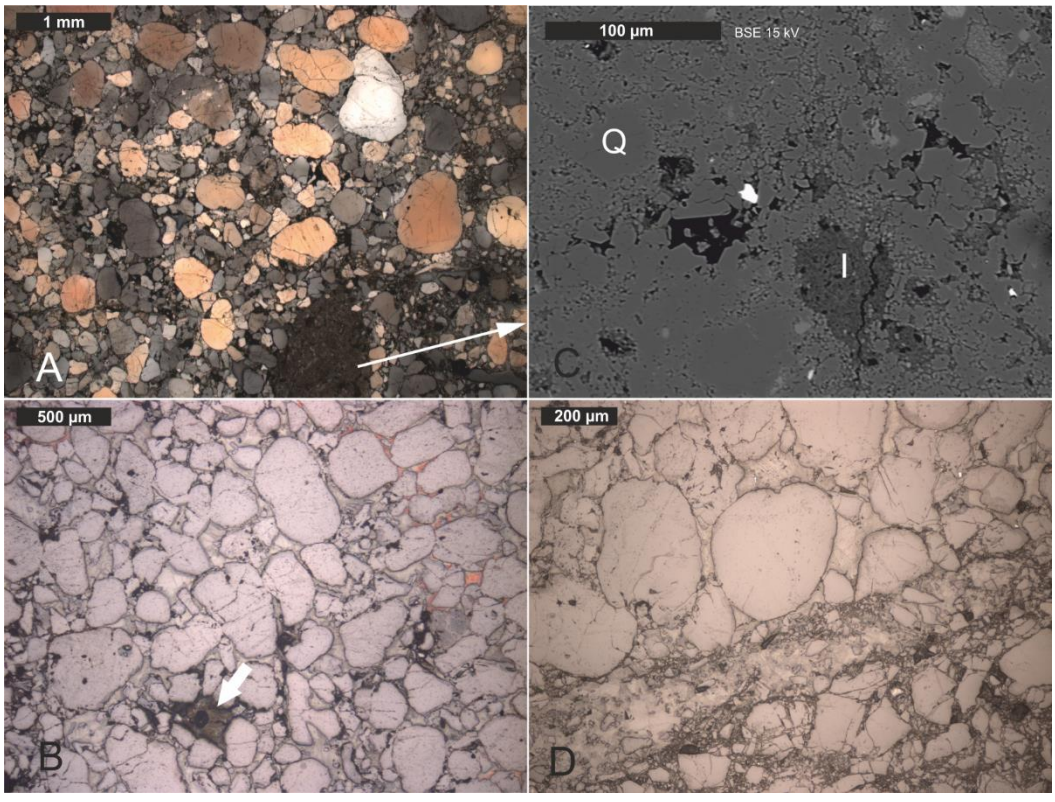
1 mm
A
100 µm
BSE 15 kV
Q
I
C
500 µm
B
200 µm
D

Fig. 8

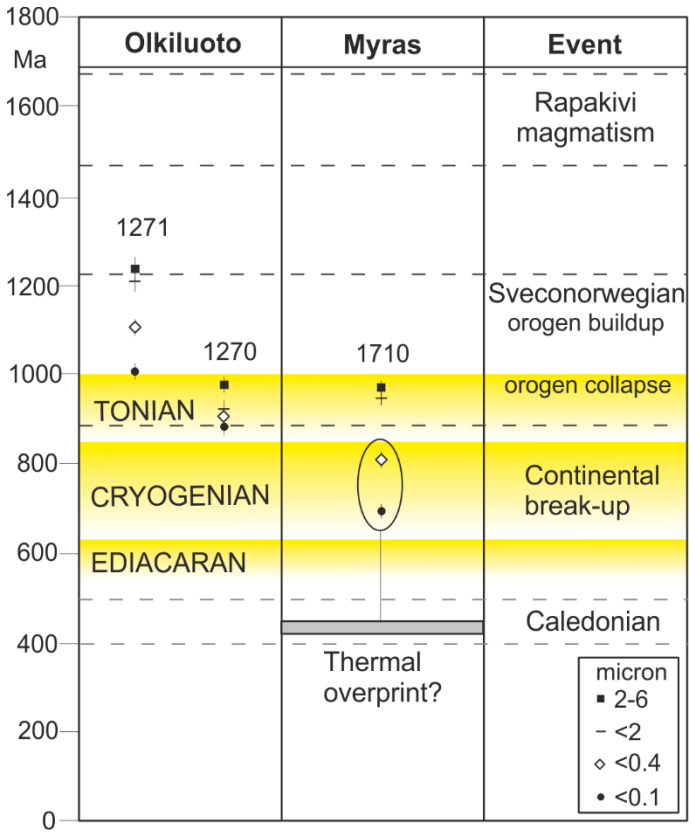
1800
Ma
1600
1400
1200
1000
800
600
400
200
0
Olkiluoto
Myras
Event
Rapakivi magmatism
1271
Sveconorwegian orogen buildup
1270
1710
orogen collapse
TONIAN
CRYOGENIAN
Continental break-up
EDIACARAN
Caledonian
Thermal overprint?
micron
2-6
<2
<0.4
<0.1

Fig. 9

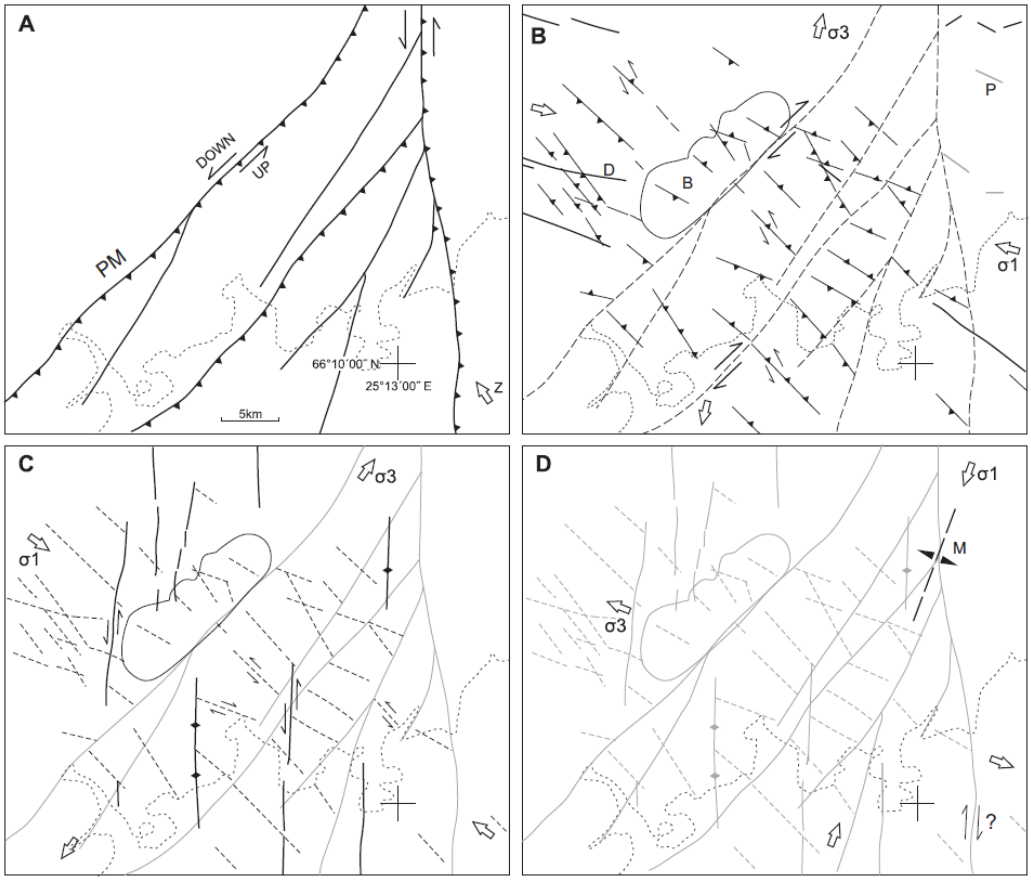
A
DOWN
UP
PM
66°10'00" N
25°13'00" E
5km
Z
B
σ3
P
D
B
σ1
C
σ3
σ1
D
σ1
M
σ3
?

Fig. 10

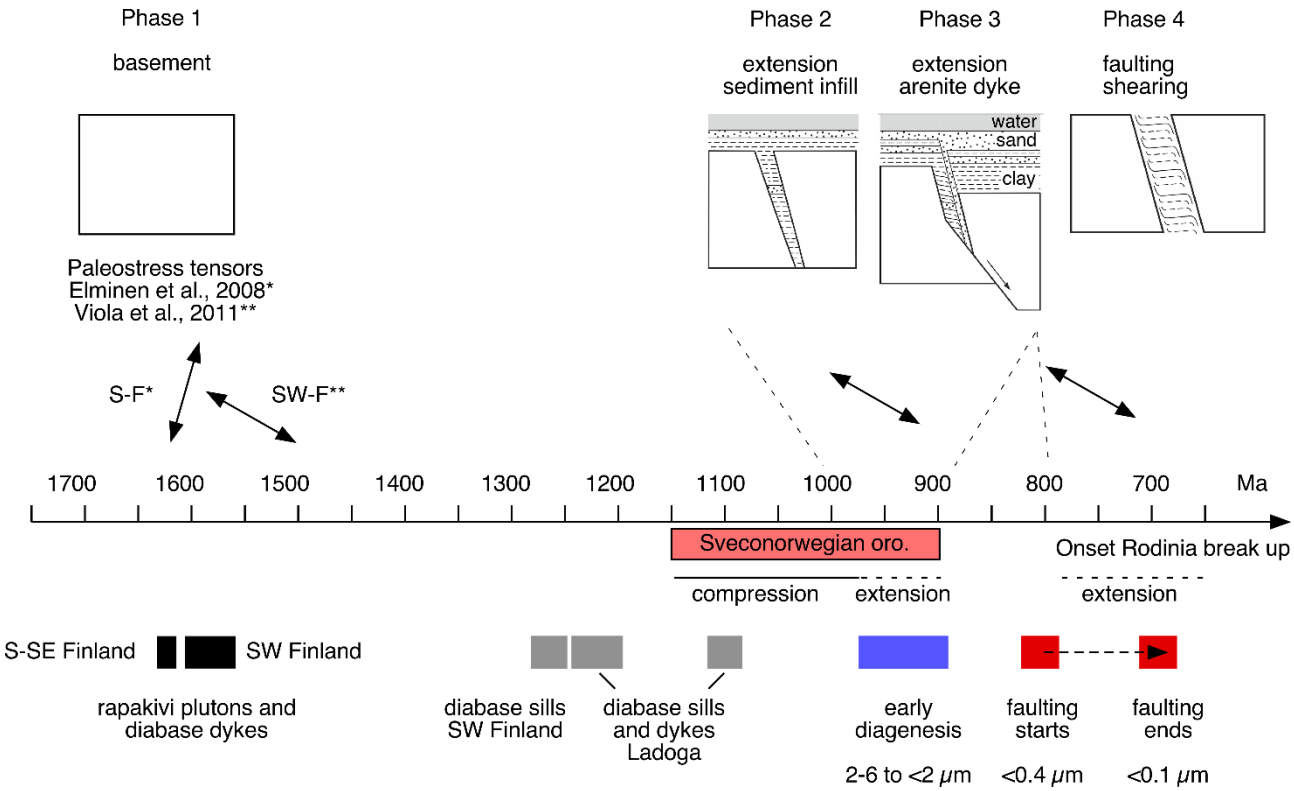
Phase 1
basement
Phase 2
extension
sediment infill
Phase 3
extension
arenite dyke
Phase 4
faulting
shearing
water
sand
clay
Paleostress tensors
Elminen et al., 2008*
Viola et al., 2011**
S-F*
SW-F**
1700
1600
1500
1400
1300
1200
1100
1000
900
800
700
Ma
Sveconorwegian oro.
Onset Rodinia break up
compression
extension
extension
S-SE Finland
SW Finland
rapakivi plutons and
diabase dykes
diabase sills
SW Finland
diabase sills
and dykes
Ladoga
early
diagenesis
2-6 to <2 μm
faulting
starts
<0.4 μm
faulting
ends
<0.1 μm

Fig. 11

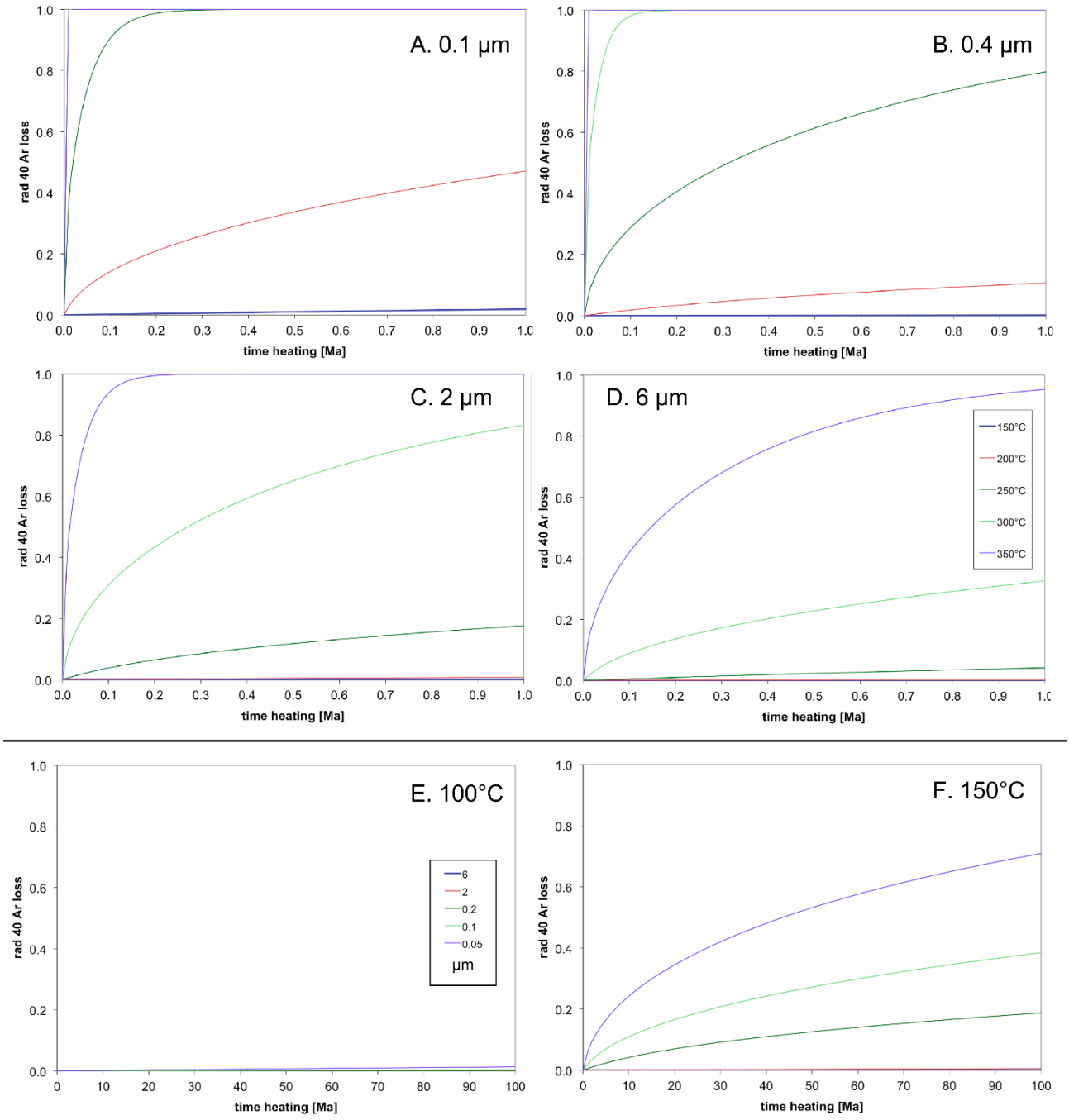
A. 0.1 µm
B. 0.4 µm
C. 2 µm
D. 6 µm
E. 100°C
F. 150°C
rad 40 Ar loss
time heating [Ma]
150°C
200°C
250°C
300°C
350°C
6
2
0.2
0.1
0.05
µm

Fig. 12

Table 1. K–Ar age standard and airshot data.

Sample ID	CSIRO ID	K [%]	Rad. 40Ar [mol/g]	Rad. 40Ar [%]	Age [Ma]	Error [Ma]	Remark
Standard	HD-B1-105	7.96	3.378E-10	93.12	24.31	0.38	Error to ref.: +0.41%
airshot	40Ar/36Ar	+/-					
AS101-AirS-1	297.06	0.37					
AS101-AirS-2	294.03	0.50					

Table 2. XRD data for the bulk sample and for separated <2 μm clay-size fractions.

Sample ID	Quartz [%]	Illite 2M1 [%]	Illite 1M [%]	Chlorite [%]	Orthoclase/Microcline [%]
TU4-38040 bulk	55	10		5	30
1710 <2μm	-	42	54	5	-

Table 3. K–Ar age data.

Sample ID [μm]	K [%]	Rad. 40Ar [mol/g]	Rad. 40Ar [%]	Age [Ma]	Error [Ma]	Period-Epoch-Stage Gradstein et al. (2004)
TU4-38040 <0.1	6.40	9.4498E-09	97.80	697.3	14.1	Neoproterozoic-Cryogenian
TU4-38040 <0.4	6.70	1.1868E-08	98.48	809.3	16.4	Neoproterozoic-Cryogenian
TU4-38040 <2	6.56	1.4172E-08	98.85	947.1	19.5	Neoproterozoic-Tonian
TU4-38040 2-6	6.78	1.5057E-08	99.15	967.6	19.7	Neoproterozoic-Tonian

Table 4. Argon diffusion data with parameters (1) grain-sizes 0.1 to 6 μm, (2) range 200–350 °C and (3) 1 My timeframe.

200°C	2-6 μm	< 2 μm	<0.4 μm	<0.1 μm
0.1 Ma	0.00	0.00	0.03	0.21
0.5 Ma	0.00	0.00	0.11	0.47
1.0 Ma	0.00	0.01	0.16	0.64
250°C				
0.1 Ma	0.01	0.04	0.41	0.99
0.5 Ma	0.02	0.12	0.80	1.00
1.0 Ma	0.04	0.18	0.94	1.00
300°C				
0.1 Ma	0.09	0.31	0.98	1.00
0.5 Ma	0.23	0.65	1.00	1.00
1.0 Ma	0.33	0.83	1.00	1.00
350°C				
0.1 Ma	0.42	0.94	1.00	1.00
0.5 Ma	0.82	1.00	1.00	1.00
1.0 Ma	0.94	1.00	1.00	1.00

Table 4. Argon diffusion data with parameters (1) grain-sizes 0.1 to 6 μm, (2) temperature range 150 to 350 °C and (3) 1 My timeframe.

200°C	2-6 μm	< 2 μm	<0.4 μm	<0.1 μm
0.1 Ma	0.00	0.00	0.03	0.21
0.5 Ma	0.00	0.00	0.11	0.47
1.0 Ma	0.00	0.01	0.16	0.64

250°C				
0.1 Ma	0.01	0.04	0.41	0.99
0.5 Ma	0.02	0.12	0.80	1.00
1.0 Ma	0.04	0.18	0.94	1.00
300°C				
0.1 Ma	0.09	0.31	0.98	1.00
0.5 Ma	0.23	0.65	1.00	1.00
1.0 Ma	0.33	0.83	1.00	1.00
350°C				
0.1 Ma	0.42	0.94	1.00	1.00
0.5 Ma	0.82	1.00	1.00	1.00
1.0 Ma	0.94	1.00	1.00	1.00